JGR Atmospheres

RESEARCH ARTICLE
10.1029/2023JD040289

Smoke with Induced Rotation and Lofting (SWIRL) Generated by the February 2009 Australian Black Saturday PyroCb Plume

D. R. Allen[1], M. D. Fromm[1], G. P. Kablick III[1], G. E. Nedoluha[1], and D. A. Peterson[2]

[1]Remote Sensing Division, Naval Research Lab, Washington, DC, USA, [2]Marine Meteorology Division, Naval Research Lab, Monterey, CA, USA

Key Points:

- The February 2009 Australian Black Saturday pyroCbs injected a smoke plume into the stratosphere that induced a mesoscale anticyclone
- The anticyclone was 1000 km across and 2 km thick and traveled 27,000 km in three weeks as it rose from 18 to 21 km in altitude
- Satellite trace gas and aerosol anomalies coincide with potential vorticity anomalies, confirming smoke-induced dynamical perturbations

Correspondence to:
D. R. Allen,
douglas.r.allen30.civ@us.navy.mil

Citation:
Allen, D. R., Fromm, M. D., Kablick, G. P., III, Nedoluha, G. E., & Peterson, D. A. (2024). Smoke with Induced Rotation and Lofting (SWIRL) generated by the February 2009 Australian Black Saturday PyroCb plume. *Journal of Geophysical Research: Atmospheres*, *129*, e2023JD040289. https://doi.org/10.1029/2023JD040289

Received 25 OCT 2023
Accepted 14 FEB 2024

Abstract The discovery of smoke-induced dynamical anomalies in the stratosphere associated with the 2019/2020 Australian New Year pyrocumulonimbus (pyroCb) super outbreak initiated a new field of study involving aerosol/weather anomalies. This paper documents the dynamical anomalies associated with the February 2009 Australian Black Saturday pyroCb outbreak. Positive potential vorticity anomalies (indicating anticyclonic rotation) with horizontal extent ∼1000 km and vertical thickness ∼2 km are associated with the plume, which we classify as a Smoke With Induced Rotation and Lofting (SWIRL). The SWIRL initially formed east of Australia, but then moved westward, crossing over Australia, and continuing to Africa. The SWIRL lasted for nearly three weeks (13 February–4 March), traveling ∼27,000 km and rising from potential temperatures of ∼410–500 K (altitudes ∼18–21 km). The altitude of the SWIRL is corroborated with coincident satellite-based profiles of H_2O, CO, HCN, O_3, and aerosol extinction. A vertical temperature dipole (±3 K) accompanied the PV anomaly, as verified with coincident Global Navigation Satellite System radio occultation temperatures. The SWIRL dissipated as it passed over Africa. Operational ECMWF forecasts with early initialization (13 February) and late initialization (21 February) are examined. In the early case, the forecasted PV anomaly disappeared within 4 days, as expected due to lack of smoke heating in the forecast model. In the late case, while the forecasted PV anomaly was weaker than in the reanalyzes, a remnant anomaly remained out to 10 days.

Plain Language Summary Large bushfires in February 2009 in Australia led to large thunderstorms called pyrocumulonimbus (pyroCb) that injected significant amounts of smoke high into the atmosphere. When this smoke was warmed by absorbing sunlight it became buoyant and started to rise and rotate. This feature has been named a Smoke With Induced Rotation and Lofting (SWIRL) and had previously been observed in large pyroCbs that occurred around New Year's Day 2020 and in Canadian fires that occurred in 2017. The February 2009 SWIRL was a pancake-like structure 1000 km across and 2 km thick. It lasted for three weeks, traveling over 27,000 km, and rising from 18 to 21 km in altitude. The SWIRL was observed both in weather maps and in satellite observations of gases such as water vapor, carbon monoxide, and ozone. Forecasting the SWIRL is difficult because current numerical weather models either do not consider smoke heating or lack inputs of pyroCb events as they are occurring in real time.

1. Introduction

The 2019/2020 Australian New Year Super Outbreak (ANYSO) of pyroCbs led to the discovery and new understanding of interactions between large smoke plumes and the atmosphere. While earlier pyroCb smoke plumes exhibited lofting related to absorption of solar radiation (Das et al., 2021; Khaykin et al., 2018; Torres et al., 2020; Yu et al., 2019), ANYSO clearly showed that the heating associated with this process was sufficient to generate anticyclonic circulation anomalies identifiable in potential vorticity from meteorological analyses (Kablick et al., 2020; Khaykin et al., 2020). This feature has been called a Smoke-Charged Vortex (SCV) (Khaykin et al., 2020; Lestrelin et al., 2021) and a Smoke With Induced Rotation and Lofting (SWIRL; Allen et al., 2020, hereafter A20). Weather models used to create the analyses described in these papers did not include smoke-induced heating, however the assimilation of temperature data resulted in the production of SWIRLs (Lestrelin et al., 2021). In the absence of smoke-induced heating, forecast models are not able to maintain these vorticity anomalies, as has been shown by Khaykin et al. (2020) with European Center for Medium-Range Weather Forecasts (ECMWF) forecasts, and by A20 for Navy Global Environmental Model (NAVGEM) forecasts.

The SWIRL discovery led scientists to examine other previous pyroCb smoke plumes for signs of anticyclonic rotation. The 2017 Pacific Northwest Event (PNE) was an obvious first choice. Khaykin et al. (2018) examined the plume using Cloud-Aerosol Lidar and Infrared Pathfinder Satellite Observations (CALIOP) lidar, Ozone Mapping and Profiling Suite (OMPS) aerosol index, and Observatoire de Haute-Provence (OHP) lidar data and showed significant lofting with time but did not look for rotation. A20 showed that one of the PNE plumes had PV anomalies in the Modern-Era Retrospective analysis for Research and Applications, Version 2 (MERRA2) analyses. More work on the PNE was performed by Lestrelin et al. (2021), who used ECMWF Reanalysis v5 (ERA5) data to examine the evolution of several vortices associated with the event. Doglioni et al. (2022) used the Goddard Earth Observing System Chemistry Climate Model (GEOS CCM) to examine how PNE aerosol injections impacted temperatures and winds. They showed that the aerosol heating was able to form and maintain synoptic-scale stratospheric anticyclones. A high-resolution (~7 km) nonhydrostatic simulation of the PNE SWIRL was performed by Guimond et al. (2023). They examined the vorticity dynamics of the plume and showed that divergence in the updraft dilutes the background absolute vorticity resulting in an anticyclonic vortex.

This paper builds upon previous work by examining a SWIRL associated with the February 2009 Australian Black Saturday pyroCbs. The large bush fires of that year produced unusually strong lofting of aerosol after injection into the stratosphere. Pumphrey et al. (2011) detailed the evolution of Microwave Limb Sounder (MLS) carbon monoxide for about a month following the pyroCb event on 7 February, showing the motion and final dissipation of an enhanced CO region associated with the event. Siddaway and Petelina (2011) further examined the transport and evolution of the smoke plume using measurements from Optical Spectrograph and Infrared Imager System (OSIRIS). de Laat et al. (2012) examined observations from multiple datasets, including Ozone Monitoring Instrument (OMI) and Global Ozone Monitoring Experiment (GOME-2) aerosol index, Atmospheric Infrared Sounder (AIRS) CO, and aerosol observations from Moderate Imaging Spectroradiometer (MODIS) and CALIOP. Further analysis by Fromm et al. (2021) of the Black Saturday plume included OMI aerosol index, MODIS imagery, MLS CO, and CALIOP. Glatthor et al. (2013) examined Michelson Interferometer for Passive Atmospheric Sounding (MIPAS) C_2H_2, HCN, and HCOOH measurements of the plume, comparing with simulations from the Global Environmental Multiscale Air Quality (GEM-AQ) model.

Although rising motion was clearly seen in several of these studies, the presence of rotation (i.e., SWIRL) for the Black Saturday event has not been documented. Using similar techniques to A20, we show that this event resulted in a SWIRL that lasted for about three weeks, and we examine its properties. We also compare the structure of the SWIRL with satellite observations of aerosol, hydrogen cyanide, carbon monoxide, water vapor, ozone, and temperature. Finally, we compare archived ECMWF operational forecasts of potential vorticity with analyses to further examine the extent to which lack of smoke heating affects the ability to predict SWIRL behavior. This paper is outlined as follows. Section 2 describes the data. Section 3 presents the SWIRL tracking method. Section 4 examines the SWIRL diagnostics, and Section 5 examines SWIRL forecasts. Section 6 provides a summary and conclusions.

2. Data Description

2.1. ERA5

PV data are derived from ERA5 reanalyzes (Hershbach et al., 2020) at 3-hourly intervals, extracted at a horizontal resolution of 0.4° longitude × 0.4° latitude over 137 model levels (native horizontal resolution is ~31 km). Relative vorticity and temperature data are used to calculate Ertel potential vorticity (Andrews et al., 1987). To reduce the impact of resolved gravity waves in the PV field, the data are horizontally smoothed with a 9-point boxcar smoothing (3.6° width). PV is examined on model levels and no vertical smoothing is applied. In addition, geopotential height on model levels is calculated from surface pressure, specific humidity, and temperature fields as described in https://confluence.ecmwf.int/display/CKB/ERA5%3A+compute+pressure+and+geopotential+on+model+levels%2C+geopotential+height+and+geometric+height.

2.2. ECMWF Operational Forecasts

We also examine two archived operational forecasts initialized on 13 and 21 February 2009 (0000 UTC for each case). The February 2009 operational forecasts use a reduced vertical resolution of 91-levels rather than 137. We extracted the data at the same 0.4° × 0.4° horizontal resolution, horizontally smoothed with a 9-point boxcar smoothing (3.6° width), and then interpolated vertically from 91-levels to the 137-levels using the 3D pressure

fields from ERA5. There is close correspondence between certain levels, so the interpolation errors are likely to be small (see https://confluence.ecmwf.int/display/UDOC/Correspondence+between+the+L91+and+L137+model+levels). We saved the archived forecasts every 24 hr out to 10 days.

2.3. OMI

To track the horizontal location of the smoke plume, we use level-3 aerosol index (AI) data from the EOS Aura Ozone Monitoring Instrument (OMI) (Bhartia, 2012; latitude × longitude resolution of 1° × 1°). These are derived with the OMI near UV algorithm using observations at 354 and 388 nm (Torres et al., 2007). Since early 2008, OMI data have experienced a row anomaly (likely due to an internal obstruction affecting the instrument's optics) that affects about half of the instrument's 60 viewing positions, reducing the possible spatial coverage (Torres et al., 2018). The row anomaly obscures some of the SWIRL features, but the dataset is still useful for corroborating the SWIRL position with high aerosol, and this row anomaly does not severely affect our conclusions.

2.4. ACE-FTS

Atmospheric Chemistry Experiment Fourier Transform Spectrometer (ACE-FTS) Version 5.2 data (Bernath et al., 2020; Boone et al., 2023) are used to examine the vertical structure of the plume, focusing on water vapor (H_2O), carbon monoxide (CO) hydrogen cyanide (HCN), and ozone (O_3). In addition, we examine the Version 5.2 1 μm extinction data from the ACE imager. ACE uses solar occultation geometry, which has high vertical resolution but limited horizontal sampling. There was one very good match with the Black Saturday SWIRL on 27 February 2009 (occultation sr29848), which was examined in Boone, Bernath, and Fromm (2020) using Version 4 data (Boone, Bernath, Cok, et al., 2020). Here we compare the V5.2 profiles with the PV analysis.

2.5. MLS

Aura MLS Version 4.2, Level 2 (L2) gas measurements are retrieved on pressure surfaces and undergo control screening for data quality, precision, and accuracy (Livesey et al., 2020). The L2 geopotential height (GPH) product is used to convert from pressure-surfaces to altitude. Carbon monoxide (CO) is retrieved using two bands observed with the 240 GHz radiometer (Pumphrey et al., 2007), and hydrogen cyanide (HCN) is retrieved using the partial band information observed near the 177.26 GHz spectral line (Pumphrey et al., 2006). CO is considered useful between 215 and 0.0046 hPa (∼11–36 km), but HCN has a reduced vertical range because of interfering lines of other species and is limited to 21–0.1 hPa (∼23–37 km) for scientifically useful data. However, HCN is retrieved down to 100 hPa, and can provide qualitative insight during anomalous conditions depending on how strong the observed deviation is from the expected value.

2.6. GNSS-RO

The Constellation Observing System for Meteorology Ionosphere and Climate (COSMIC-1) was launched 14 April 2016 with six satellites in 72-degree inclination orbit. Global Navigation Satellite System radio occultations (GNSS-RO) are processed to obtain temperature profiles. We examine a level 2 "dry temperature" profile from the 2021 reprocessed version available on the CDAAC (COSMIC, 2002).

2.7. CALIOP

CALIOP is a two-wavelength polarization lidar on board the Cloud-Aerosol LIDAR and Infrared Pathfinder Satellite (CALIPSO) mission that measures aerosols and clouds in the troposphere and lower stratosphere (Winker et al., 2009). We use the total attenuated 532 nm backscatter level 1 product, available at https://doi.org/10.5067/CALIOP/CALIPSO/CAL_LID_L1-Standard-V4-51.

3. PV Tracking Method

The PV tracking method used in this paper is based on the method described in A20 for the ANYSO event plumes (a similar tracking approach was used by Lestrelin et al. (2021) to analyze both ANYSO and PNE plumes). A summary is provided here, along with new features developed for the Black Saturday analysis. The plume identification is based on PV calculated from the ERA5 vorticity and temperature fields. PV is calculated at each model level k and grid point as $q(\lambda,\varphi,k,t)$, where λ, φ, and t refer to longitude, latitude, and time, respectively.

Tracking uses 3-hr intervals from 13 February 2009 (0000 UTC) to 4 March 2009 (0000 UTC) for a total of 153 times.

The primary diagnostic quantity is the PV anomaly, q', where prime indicates anomaly,

$$q'(\lambda,\varphi,k,t) = \frac{q(\lambda,\varphi,k,t) - \overline{q}(\varphi,k,t)}{|\overline{q}(\varphi,k,t)|} \times 100\% \quad (1)$$

where the overbar indicates zonal mean. While in A20, q' was calculated on potential temperature (θ) surfaces, here we calculate q' on model levels (hybrid sigma-pressure) to avoid the potential loss of information in interpolation. This is important especially for features that have small vertical scales. The maximum q' is next found at each model level within a horizontal search region.

$$q'_{\max}(k,t) = \max\left[q'(\lambda,\varphi,k,t)\right] \quad (2)$$

within the region defined by longitude and latitude bounds:

$$\left[\lambda_{min}(t),\lambda_{max}(t),\varphi_{min}(t),\varphi_{max}(t)\right]. \quad (3)$$

We use a region of size $d\lambda = \lambda_{max} - \lambda_{min} = 20^{\circ}$ and $d\varphi = \varphi_{max} - \varphi_{min} = 10^{\circ}$, centered on the SWIRL centroid position, $\lambda_c(t)$,$\varphi_c(t)$, calculated from the previous time step. The search region therefore adaptively tracks the SWIRL as it is advected by the ambient winds. Since we are using a relatively short 3-hr time step, the centroid is not advected very far in one time step and this simple tracking method works well. We manually picked the initial search region location by examining q' and OMI AI maps.

As an illustration of the approach, Figure 1 shows q' for 18 February 2009 (0000 UTC) at 8 model levels that span in θ from ~420 to 480 K. The search region is plotted and the q_{fmax} location is indicated by the black dots on each level. A coherent approximately oval-shaped q' feature is seen north of New Zealand at levels 50 through 54. The black contour surrounding this feature is the cutoff value $q' = 30\%$, described further below. Other positive q' features are present at some levels, which could cause problems if a larger search region is used.

The SWIRL centroid vertical level is determined from the maximum value over the given vertical search range:

$$k_c(t) = \text{where}\left[\max_{k_{\min},k_{\max}}\left(q'_{\max}(k,t)\right)\right] \quad (4)$$

and the horizontal coordinates of the centroid, $\lambda_c(t)$ and $\varphi_c(t)$, are determined by the location of the q_{fmax} at level $k_c(t)$. In addition, the centroid location in θ and geopotential height (Z) are saved as $\theta_c(t)$ and $Z_c(t)$. The vertical search range is limited to the ERA5 model levels that are bounded by $\theta_{min}(t)$ and $\theta_{max}(t)$. These start with the values 390 and 550 K, respectively. Over time, as the plume rises, the minimum bound is allowed to increase to the value of $\theta_c(t)$-30 K but is not allowed to decrease. This is to avoid spurious anticyclonic features that could occur at lower altitudes.

To identify whether q'_{max} is significantly above the background q' values, we calculated the standard deviation of q' over all longitudes but bounded by the search region latitudes. This was done separately at each model level of the vertical search range and then vertically averaged, and time averaged from 18 February to 4 March 2009. The mean standard deviation was on the order of $\sigma \sim 10\%$. We identify a q' feature to be classified as a SWIRL if the PV anomaly is greater than a cutoff value of three times the standard deviation: $q'_{max} > 3\sigma = 30\%$ and lies within the vertical search range. Table 1 compiles SWIRL information for each day at 0000 UTC.

Examples of vertical profiles of q'_{max} are provided in Figure 2 (the red lines and blue lines are temperature anomalies, which will be discussed further below), and the green lines indicate the vertical search range. Figure 2a shows the SWIRL on 13 February 2009, with a centroid level $k_c = 55$ and $q'_{max} = 82.3\%$. Figure 2b shows rising of the plume by 18 February with q'_{max} values exceeded 30% at five ERA5 model levels (50–54), and $k_c = 52$ indicating the centroid level. A similar plot is shown in Figure 3 of Siddaway and Petelina (2011) for 19 February 2009 using OSIRIS radiance data. The approximate vertical width of the dynamical anomaly associated with the

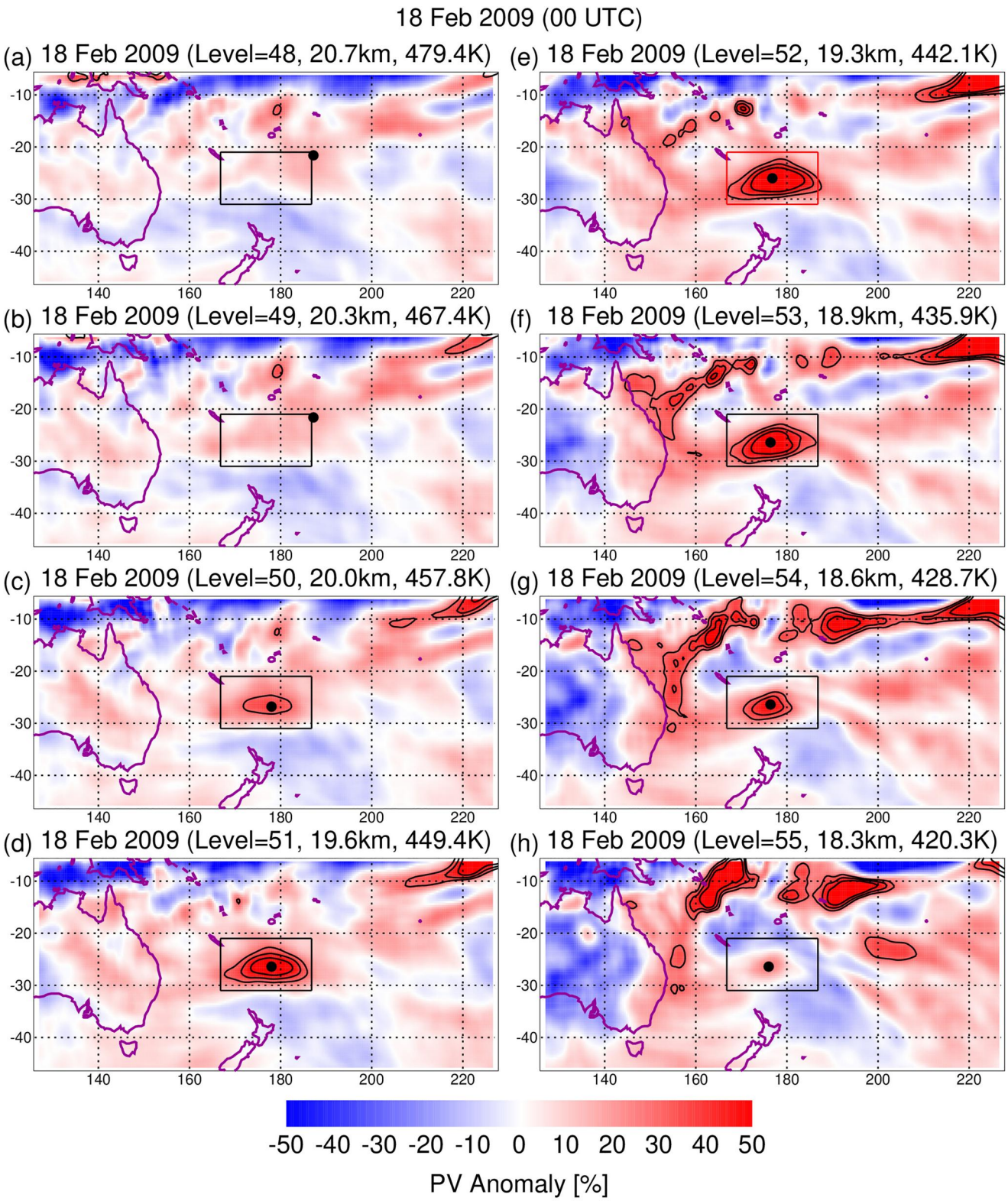

Figure 1. ERA5 PV anomaly maps for 18 February 2009 (0000 UTC) at model levels 48–55. Black contours indicate values of 30%, 40%, and 50%. Boxes indicate the search region for this time and are color-coded as red for the plume centroid level (52 in this case) and black otherwise. Black dots indicate the horizontal position of the maximum PV anomaly within the search region at each level. Altitude and θ at the location of the maximum PV anomaly are provided.

Table 1
SWIRL Centroid Information Including Date, Longitude, Latitude, Level, Altitude, θ, and PV Anomaly fo Each Day From 13 February 2009 to 4 March 2009 (0000Z for Each Day)

Date	Longitude	Latitude	Level	Alt [km]	Theta [K]	q′ [%]
13-Feb	183.2	−31.2	55	18.4	412.0	82.3
14-Feb	184.4	−31.2	54	18.6	420.8	76.3
15-Feb	189.2	−30.4	54	18.6	426.4	73.3
16-Feb	188.8	−29.6	54	18.6	430.1	68.2
17-Feb	182.0	−28.4	52	19.3	441.8	73.1
18-Feb	176.8	−26.0	52	19.3	442.1	68.7
19-Feb	168.0	−23.2	51	19.6	447.7	70.9
20-Feb	156.8	−20.4	51	19.6	448.8	69.6
21-Feb	144.0	−20.0	50	19.9	457.9	72.7
22-Feb	131.2	−19.6	49	20.3	468.1	75.6
23-Feb	119.2	−19.2	49	20.3	469.2	72.7
24-Feb	109.2	−20.4	49	20.3	466.4	77.0
25-Feb	99.2	−20.4	49	20.3	467.3	69.2
26-Feb	88.0	−18.4	49	20.3	469.1	68.7
27-Feb	77.6	−18.0	48	20.7	481.2	57.0
28-Feb	66.8	−17.6	48	20.7	487.5	48.0
1-Mar	55.6	−16.8	48	20.7	486.4	53.3
2-Mar	43.6	−16.0	47	21.0	492.7	44.1
3-Mar	28.4	−17.6	47	21.1	494.6	40.5
4-Mar	11.6	−21.2	47	21.1	497.6	29.5

plume is only ∼2 km on 18 February, which is thinner than the main ANYSO plume analyzed by A20 that had a peak thickness of ∼5–6 km. Siddaway and Petelina (2011) stated that the smoke signature for Black Saturday plume had a vertical thickness up to 6 km. The PV anomaly apparently is confined to the central part of the plume. The plume continues to rise from 23 February to 3 March (Figures 2c–2e) with the centroid level θ_c increasing from ∼470 to 495 K. On 3 March, the q'_{max} has weakened to 40.5% and is has broadened significantly.

A summary plot of q'_{max} as a function of θ and time is plotted in Figure 3a. The small black dots in Figure 3a represent θ_c, and these show a progressively rising plume, with a mean heating rate ($d\theta/dt$) of ∼4.5 K day^{-1}. This heating rate is slower than that shown in A20 for the P1 plume of the ANYSO event (∼6–8 K day^{-1}). There appears to be some diurnal variability in the location of θ_c (e.g., from 23 to 24 February), which may be due to a diurnal heating rate cycle. This feature was shown in model simulations of a PNE SWIRL described in Doglioni et al. (2022), and a similar suggestion was also made in Torres et al. (2020). However, since the amplitude of this apparent diurnal variability (∼10 K) is on the same order as the model spacing in θ (∼10 K, see Figure 2), we hesitate to draw any definite conclusions about diurnal variability from this analysis.

Figure 3b plots the horizontal location of the SWIRL, which shows initial eastward movement followed by steady westward movement from Australia to Africa. The change in motion as the SWIRL rises is similar to what was seen in the main portion of the ANYSO plume, although that plume traveled eastward to South America before reversing direction (Kablick et al., 2020). The difference is likely due to the steering winds that are driving the SWIRL bulk motion. These positions are generally similar to those shown in Siddaway and Petelina (2011) The great circle distance traveled is ∼27,000 km. The following section examines SWIRL evolution in more detail.

4. SWIRL Evolution

To summarize this section, the SWIRL is seen as a robust feature for about three weeks, from 13 February to 4 March 2009, with anticyclonic rotation and rising. Its location in the horizontal and vertical are confirmed with independent observations of trace gas, aerosol, and temperature.

4.1. 6–13 February

Figure 4 details the dynamical situation from 6 to 13 February, while the SWIRL was forming. PV anomaly at level 55 (note: θ_c = 412.0 K on 13 Feb) is plotted along with geopotential height anomaly Z' (black contours). A relatively weak high-pressure system extended from Australia to New Zealand on 6 February, accompanied by positive q', which strengthened over the next 3 days. The ambient anticyclonic circulation likely helped maintain the smoke (which was injected on 7 February) in a localized region, while at the same time, the smoke absorption of radiation could have enhanced the circulation. From 9 to 13 February, the anticyclone weakened somewhat, but a clear region of positive q' on 13 February remained, forming the core of the SWIRL centered northeast of New Zealand. A region of enhanced CO was observed in this region on 12–13 February, as shown in Figure 1 of Pumphrey et al. (2011). We note that Fromm et al. (2021) quoted a "day after" height of ∼16–17 km, (θ ∼ 374–386 K) for the Black Saturday SWIRL, so this feature likely rose diabatically prior to our discernment of an isolated SWIRL on 13 February at 18.4 km (θ_c = 412 K). While the PV anomaly shown here for the SH is positively signed, SWIRLs (in both hemispheres) are characterized by lower absolute PV. Lestrelin et al. (2021) suggest the anticyclone may be caused by pyro-convective transport of low absolute value PV tropospheric air into the higher absolute value PV stratospheric environment. Shah and Haynes (2023) provide another explanation for the low absolute PV anomaly. Using axisymmetric modeling simulations, they show that an upward-moving localized heating source results in a single-signed anticyclonic vortex co-located with the heating source

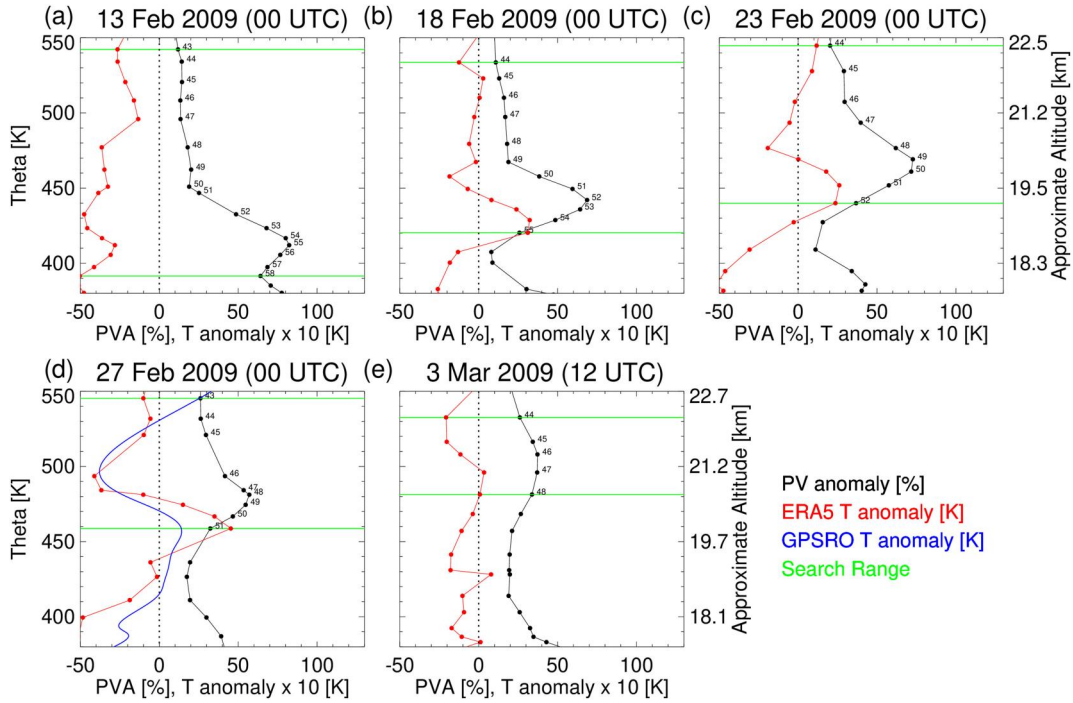

Figure 2. ERA5 PV anomaly maximum (black lines, in %) as a function of potential temperature for 13, 18, 23, 27 February 2009 (0000 UTC for each case) and 3 March 2009 (1200 UTC). Green lines indicate the minimum/maximum bounds for the automated tracking and numbers indicate the model levels. Red lines are the ERA5 temperature anomaly multiplied by 10 (in K). Blue line is the GNSS-RO temperature anomaly multiplied by 10 (in K).

in addition to a cyclonic vortex below that is not maintained by any real forcing and therefore likely decays due to radiative and mixing processes.

4.2. 13–20 February

Horizontal q' maps for the subsequent week (13–20 February) are shown in Figure 5. Considering the shape to be approximately ellipsoidal, on 13 February it is quite broad in both the major and minor axes. By 15–16 February, it becomes highly elongated, with the major axis oriented in the zonal direction. From 17 to 20 February the SWIRL axes apparently rotate in a counterclockwise direction, so by 20 February the major axis is in the southwest-northeast orientation. This shows that while the SWIRL is a robust feature, it is significantly modulated by ambient flow. A20 discussed how the tilting and rotation of the vortex can help to stabilize it against the ambient shear flow. Daily vertical (longitude/θ) q' cross-sections for 13–20 February are shown in Figure 6, slicing through the SWIRL centroid longitude and latitude. On 13 February, the positive q' is still connected to elevated q' at lower levels, but over the next two days, the SWIRL detaches from the ambient q' and becomes an isolated circulation feature on 15 February. The vertical extent of the PV anomaly on this day is ~50 K (~2 km). While initially the SWIRL extent was ~20° in longitude, it narrowed with time, forming an anomaly ~10° in longitude by 20 February. This is due to the rotation of the major axis shown in Figure 5h. The horizontal extent of the plume based on 10° width is ~1000 km, similar to the size of the main plume in the ANYSO event (A20).

To further illustrate the relationship between PV anomaly and smoke, we plot in Figure 7 the CALIOP lidar 532 nm attenuated backscatter cross section through the plume on 14 February, along with ERA5 PV anomaly contours. As shown in Figure 5b, the CALIOP measurement track is off the east coast of New Zealand. On this date, the plume extends vertically from ~400 to 450 K. PV anomaly contours closely correspond to the location of the smoke plume, with the 20% level approximately marking the plume boundary.

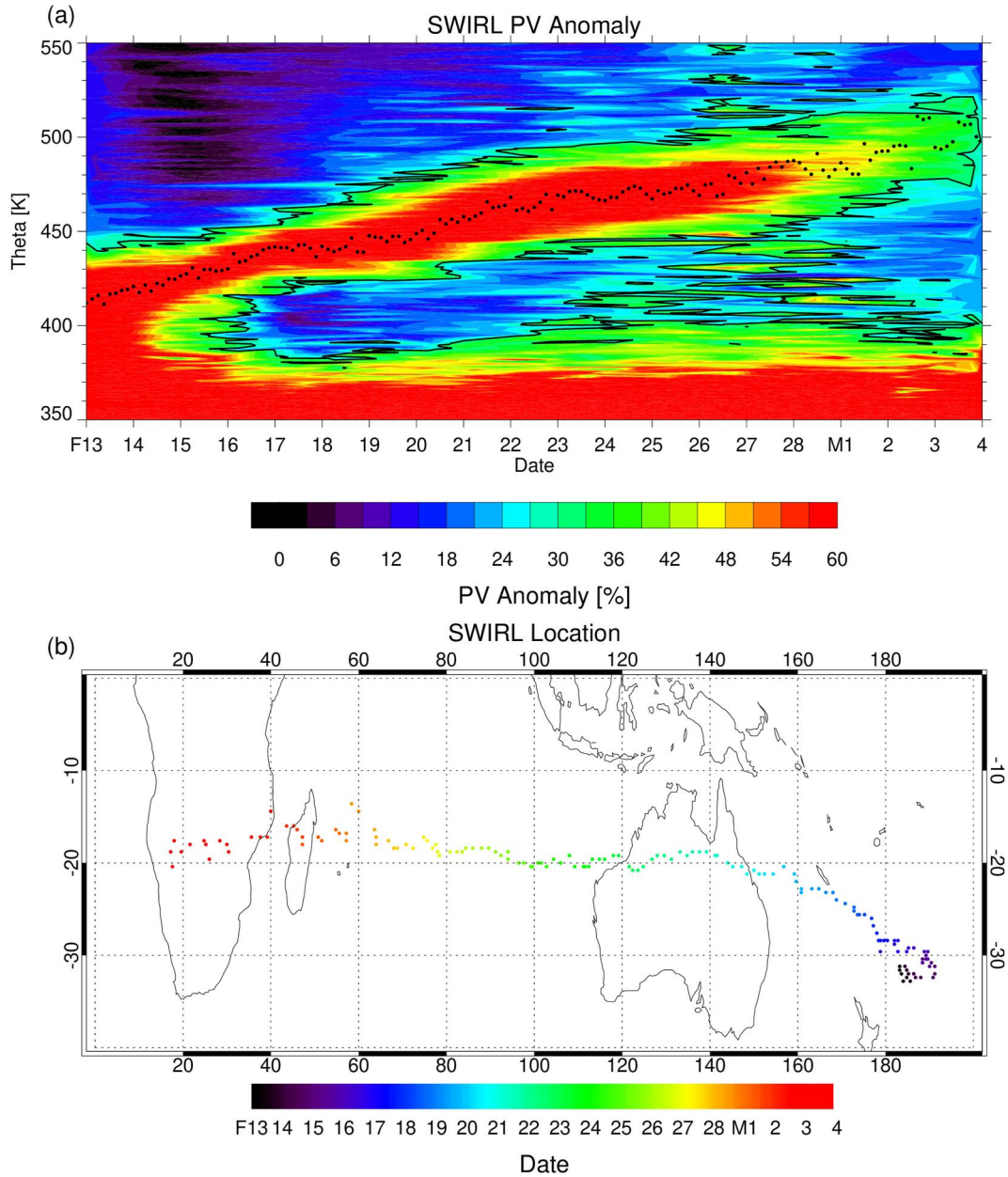

Figure 3. (a) PV anomaly maximum as a function of potential temperature for 18 February 2009 (0000 UTC) to 4 March 2009 (1200 UTC). Black dots indicate the centroid potential temperature, while black lines indicate the 30% cutoff threshold for SWIRL identification. (b) The longitude/latitude locations of the SWIRL over the same time range as in (a). Date is indicated by the color of the dots.

The dynamical structure of the SWIRL is further examined in a composite latitude/θ cross-section in Figure 8. To reduce noise, we first time averaged the PV, temperature, and zonal wind over nine 3-hourly fields from 17 February (1200 UTC) to 18 February (1200 UTC). Since the SWIRL doesn't move very much in this 24-hr period we did a straight average of the ERA5 data without shifting position. Some slight smearing might be expected in the zonal direction. We then calculated deviations from the composite time-averaged zonal mean. The plot is centered on the SWIRL centroid latitude and longitude (26.0°S, 176.8°E) for 18 February (0000 UTC). The $q'_{max} > 50\%$ in this plot, and is centered near 450 K. The zonal wind anomaly (green contours) exceeds 6 ms^{-1} eastward at 30°S and is ~6 ms^{-1} westward at 19°S, indicating anticyclonic (counterclockwise in the Southern Hemisphere) rotation. Wind anomalies are ~1/3 those of the main ANYSO plume, which maximized >15 ms^{-1}

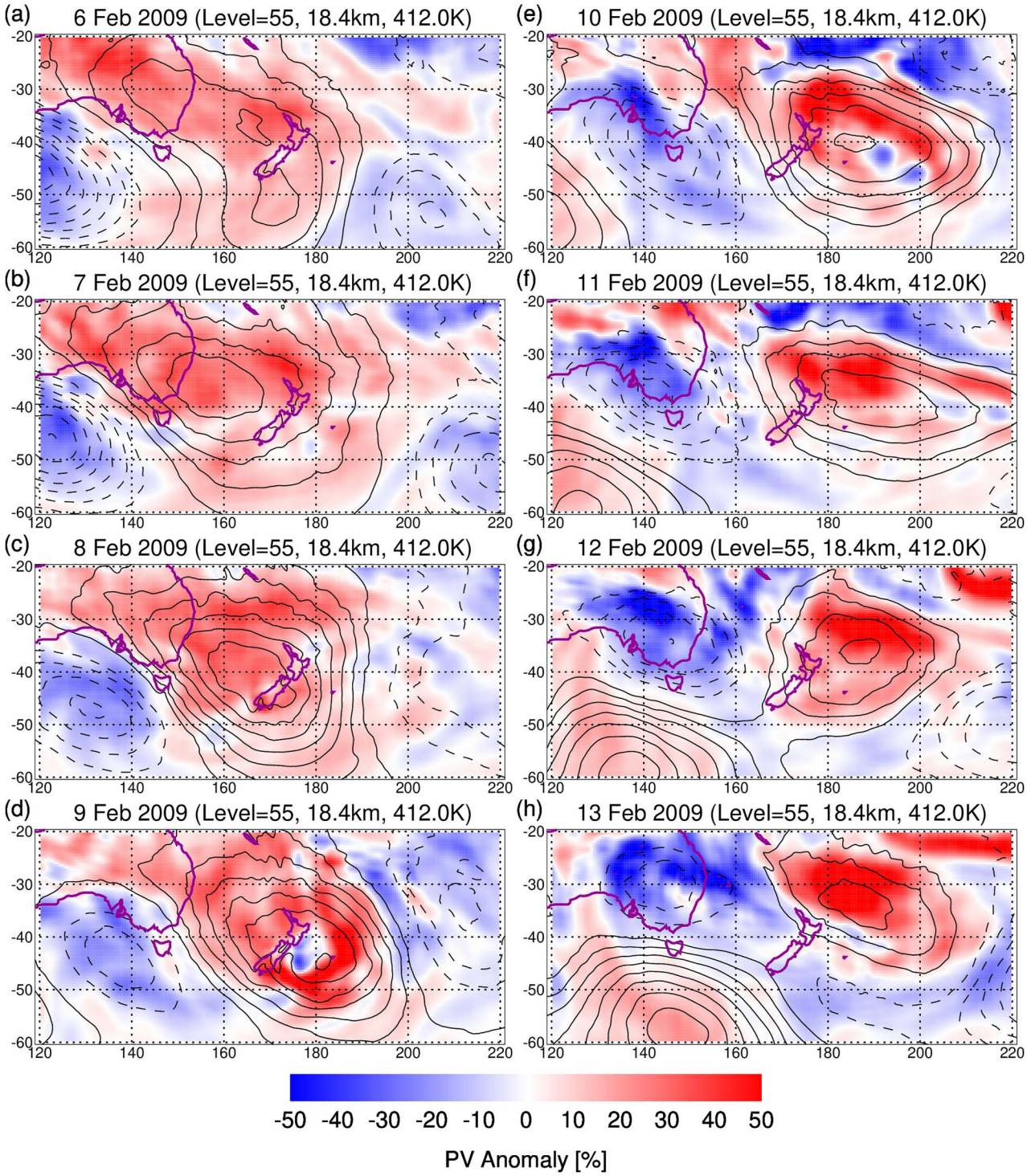

Figure 4. ERA5 PV anomaly maps for 6–13 February 2009 (0000 UTC for each case) at model level 55. Black contours are the geopotential height anomaly at 25 m intervals. Positive (negative) anomaly is plotted with a solid (dashed) line. Altitude and θ at the centroid location for 13 February 2009 (when SWIRL tracking started) are provided on each panel for reference.

(see Figure 2b of A20 and Figure 3a of Kablick et al., 2020). A temperature dipole occurs (black contours), with ~3 K warm (cold) anomaly below (above) the location of q'_{max}. This temperature dipole has been observed in other SWIRLs (e.g., Figure 2b of A20). In the main ANSYO plume the dipole showed anomalies up to ± 9 K

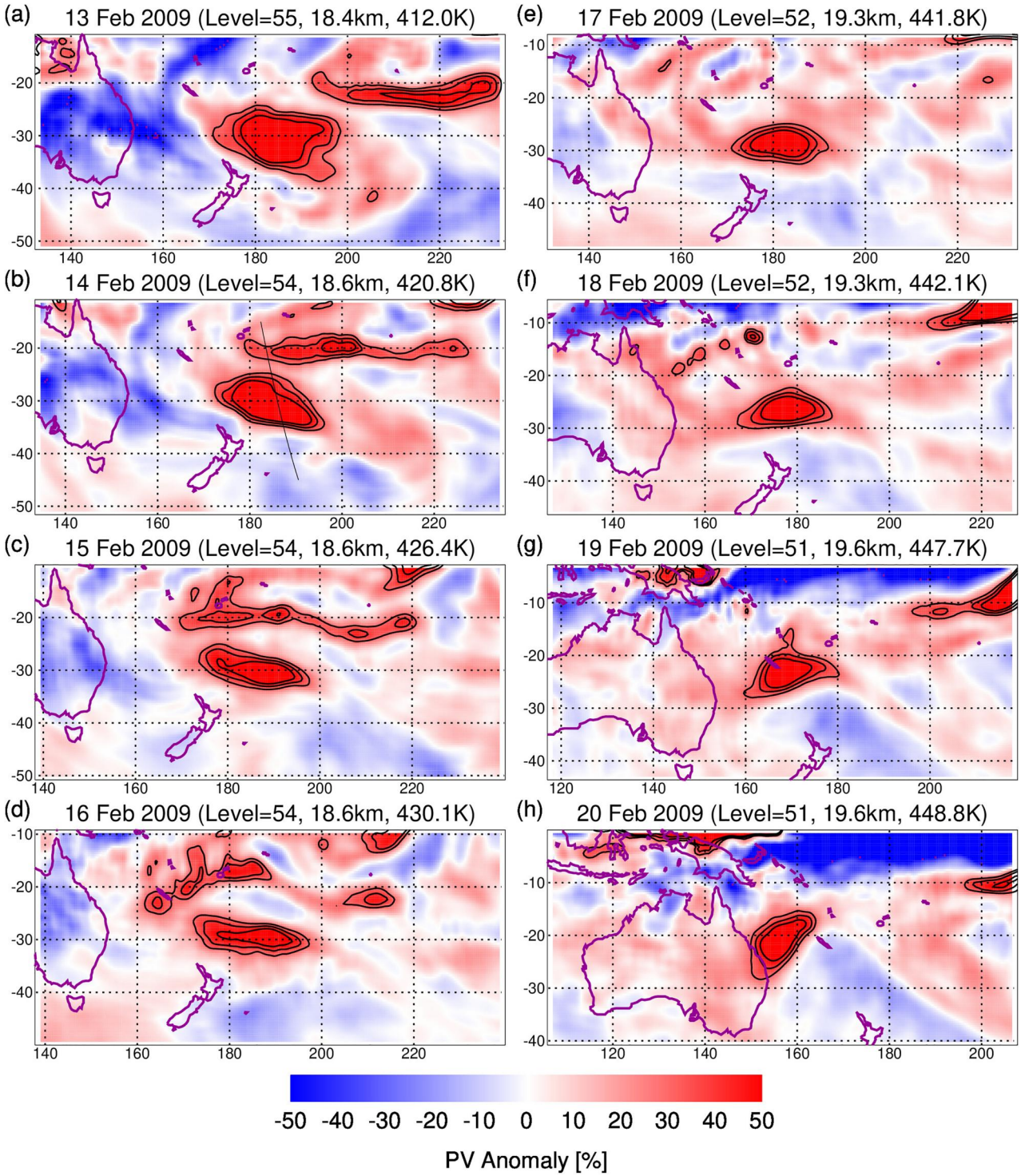

Figure 5. ERA5 PV anomaly maps for 13–20 February 2009 (0000 UTC for each case) at the centroid model level for each time. Altitude and θ at the centroid location are provided. Black contours indicate values of 30%, 40%, and 50%. The black line on panel (b) indicates the location of the CALIOP measurement track used for Figure 7.

(Kablick et al., 2020; Khaykin et al., 2020). In Figure 2, individual T' profiles from ERA5 are provided for several dates (red lines). These show generally warmer air just below the PV anomaly peak and colder air above. Overall, the structure is similar to that seen in other SWIRL composites (e.g., Lestrelin et al., 2021).

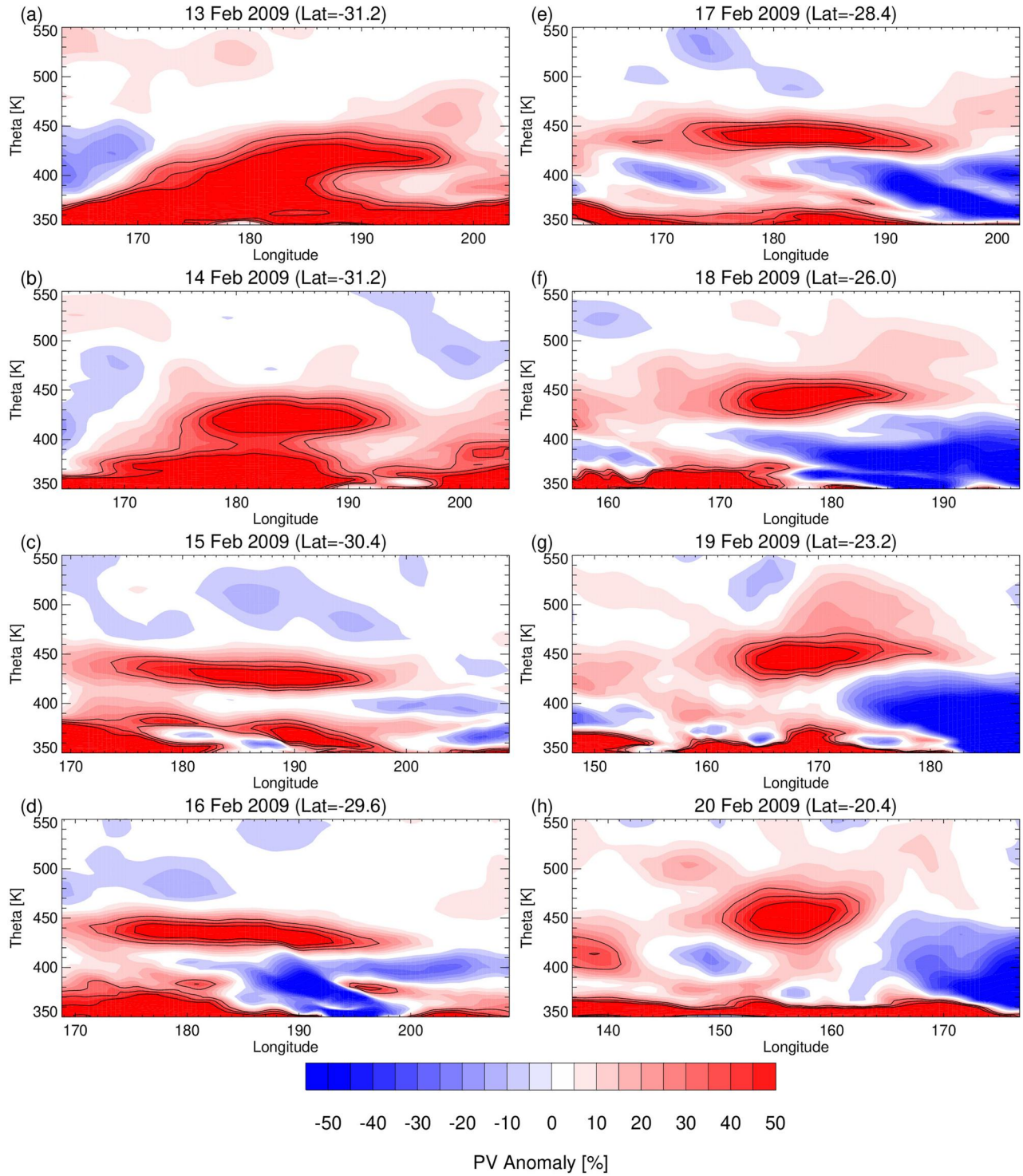

Figure 6. ERA5 PV anomaly as a function of longitude and potential temperature for 13–20 February 2009 (0000 UTC in each case) at the centroid latitude for each date. Black contours are values of 30%, 40%, and 50%.

4.3. 21–28 February

Figure 9 shows q' longitude/θ cross-sections for 21–28 February. The SWIRL continues rising over this period and maintains a relatively ellipsoidal shape until the last two days, when the size of the SWIRL, indicated by the

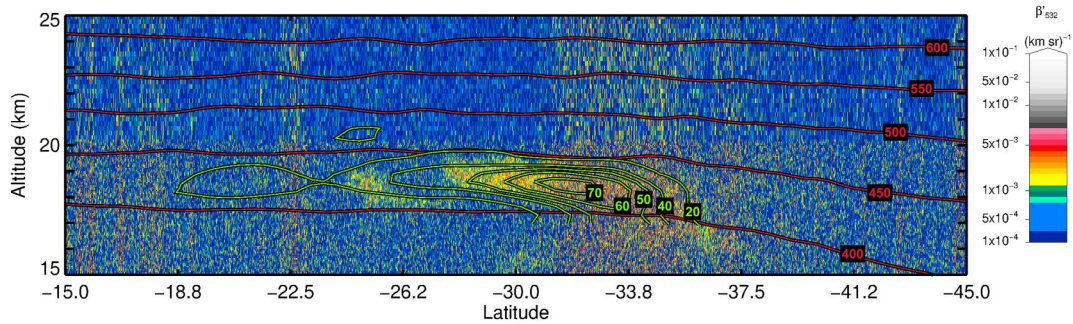

Figure 7. CALIOP 532 nm total attenuated backscatter (km^{-1} sr^{-1}) on 14 Feb 2009 for a daytime track that passed through the Black Saturday SWIRL. Red lines are potential temperature (K), and green lines are ERA5 PV anomaly (20%, 40%, 50%, 60%, and 70%) on 14 Jan 2020 (0000 UTC), for the range of potential temperatures ≥380 K. Bottom of plot indicates latitude positions along the track (which is shown in Figure 5b).

30% cutoff contour, diminishes rapidly. These cross-sections suggest that the SWIRL has a localized circulation that helps to constrain the pyroCb aerosol. The co-location of aerosol and PV anomalies was clearly shown in previous work (A20, Kablick et al., 2020; Khaykin et al., 2020, Lestrelin et al., 2021). Here, we verify this for the Black Saturday case using the OMI AI data, which are provided along with q' maps in Figure 10. Regions of missing data (e.g., due to the OMI row anomaly and orbital gaps) are indicated by hatch marks. These contribute to the apparent deformation of the aerosol feature (and associated open contours), causing some difficulty in this comparison (e.g., on 26 February). Generally, there is close correspondence of the AI contours to the location of the PV anomalies, even as the SWIRL changes shape over the course of its evolution. Some slight differences in position are likely due to differences in OMI overpass times relative to the plotted ERA5 analyses. While the SWIRL is roughly circular from 21 to 24 February, it starts to elongate and weaken from 25 to 28 February, as it crosses over the Indian Ocean. By 28 February, as it encroaches on Madagascar, the major axis of the SWIRL is nearly in the east-west direction.

On 27 February (0000 UTC) a solar occultation observation from ACE-FTS was made almost exactly at the SWIRL centroid position (see black dot on Figure 10g). Boone, Bernath, and Fromm (2020) examined multiple

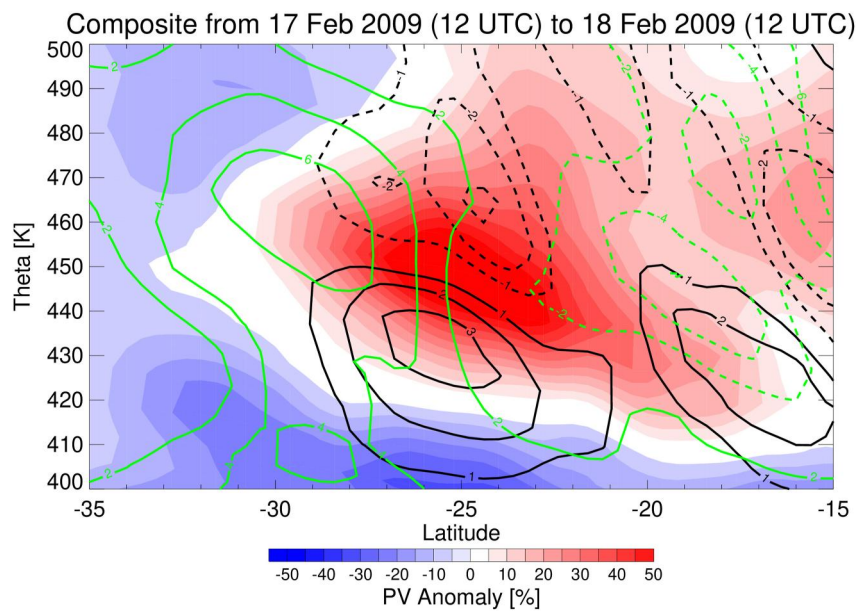

Figure 8. Composite SWIRL diagram as a function of latitude and potential temperature averaged between 17 February 2009 (1200 UTC) and 18 February 2009 (1200 UTC). Colored filled contours are the PV anomaly, black contours are temperature anomaly at ± 1, ± 2, and ± 3 K. Positive (negative) values are solid (dashed). Green contours are zonal wind anomaly at ± 2, ± 4, and ± 6 ms^{-1}. Positive (negative) values are solid (dashed).

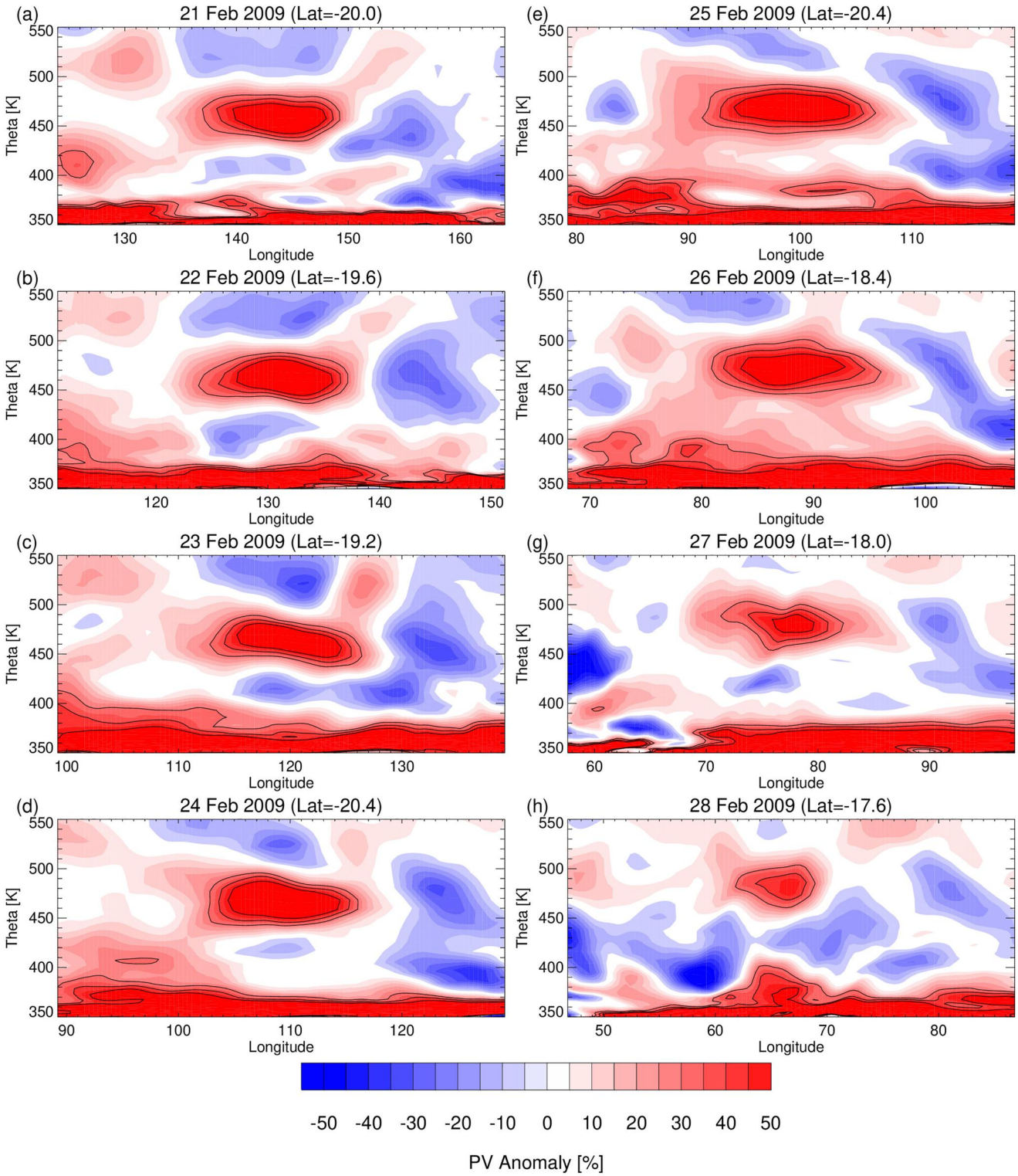

Figure 9. ERA5 PV anomaly as a function of longitude and potential temperature for 21–28 February 2009 (0000 UTC in each case) at the centroid latitude for each date. Black contours are values of 30%, 40%, and 50%.

biomass burning products for this occultation using Version 4 data, showing significant enhancements, peaking at 20 km. We use the Version 5.2 data to verify the location of the SWIRL vertical centroid position and compare with other background profiles. Pumphrey et al. (2011) examined MLS HCN and CO for the Black Saturday case,

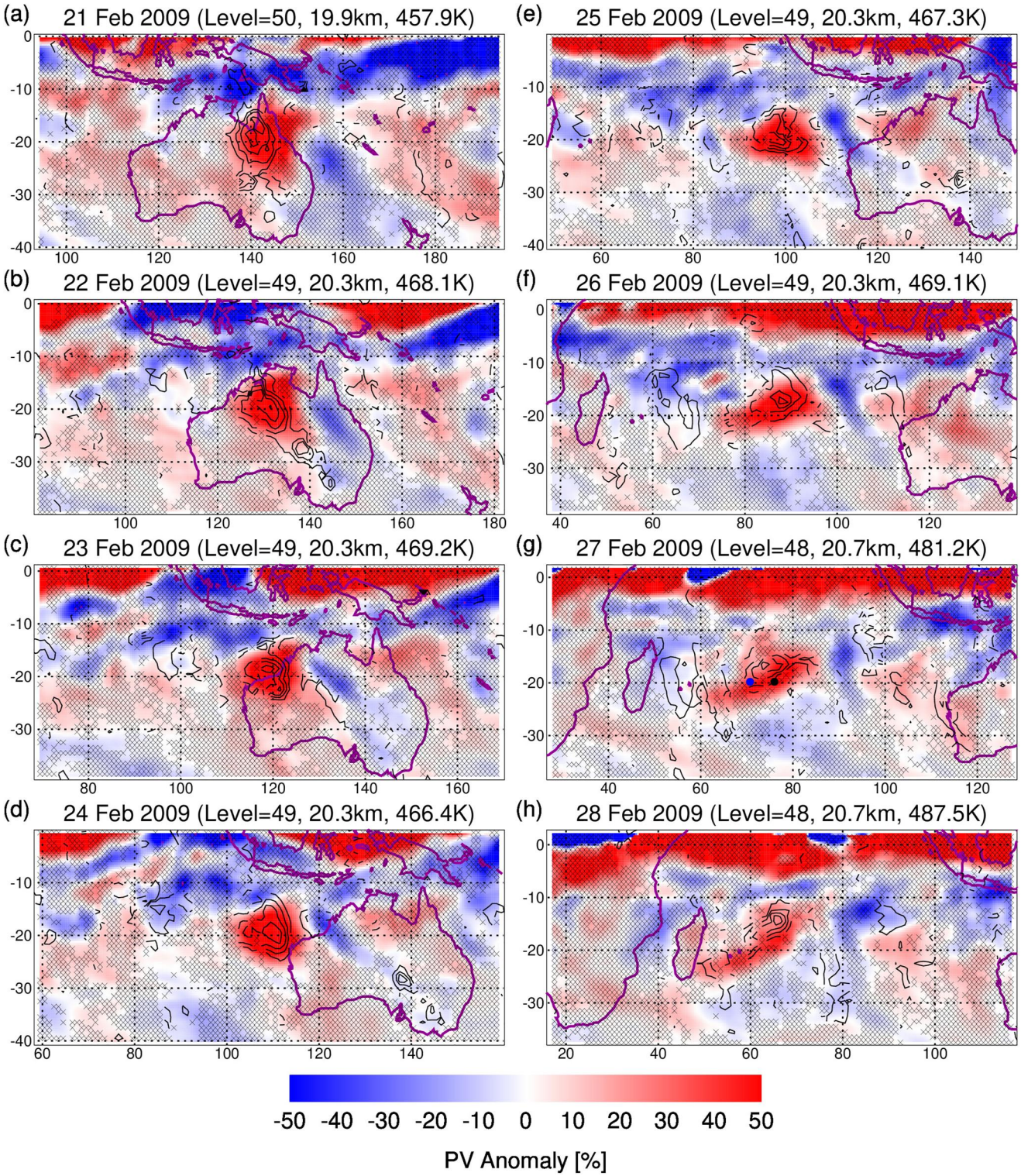

Figure 10. ERA5 PV anomaly maps for 21–28 February 2009 (0000 UTC for each case) at the centroid model level for each time. Altitude and θ at the centroid location are provided. Black contours are OMI AI values of 0.5, 1.0, 1.5, 2.0, 2.5, and 3.0. Hatched areas are regions where the OMI data are flagged as missing data. Black dot on 27 February 2009 indicates the location of the ACE-FTS occultation sr29848, which is examined in Figure 11. Blue dot on 27 February 2009 indicates the location of the GNSS-RO profile that is plotted in Figure 2d.

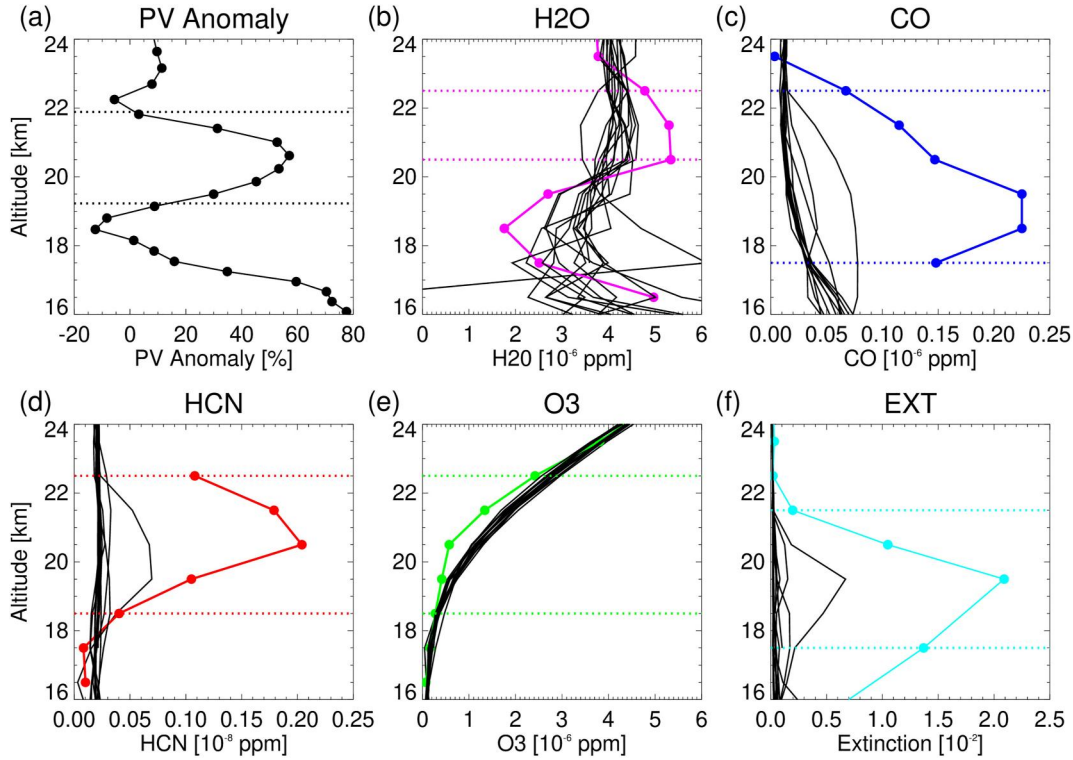

Figure 11. (a) ERA5 PV anomaly maximum (black) as a function of altitude for 27 February 2009 (0000 UTC). Dotted lines indicate enhanced anomaly. (b)–(f) ACE-FTS mixing ratios for H_2O, CO, HCN, and O_3, and (f) ACE extinction profiles. Colored solid lines are from the ACE occultation sr29848 at the location indicated by the black dot on Figure 10g. The black lines in (b)–(f) are for other ACE profiles on 26 and 27 February 2009, and the dotted lines indicate vertical ranges with values clearly above the background for H_2O, CO, HCN, and extinction and below the background for O_3.

among other species, showing significant enhancements within the polluted air mass. We examine these two species along with H_2O, O_3, and aerosol extinction. Schwartz et al. (2020) showed anomalous trace gas signatures in these species for the ANYSO event along with HNO_3 and additional biomass-burning products (CH_3Cl, CH_3CN, and CH_3OH).

Figure 11a plots $q_{f_{max}}$ as a function of altitude, showing a centroid at 20.7 km. The ACE-FTS H_2O, HCN, and CO profiles and the ACE imager extinction profile exceed the background over multiple levels, peaking at ∼19–21 km, in close alignment with the PV analysis. The ACE CO and aerosol extinction profiles peak at one retrieval level lower than the H_2O and HCN. The composition of this occultation was so optically thick that it caused instrument pointing to jump as it passed through it, which causes the discrepancy seen in peak altitude between different species (Chris Boone, personal communication, 13 September 2023). Note also that the H_2O and HCN profiles are cutoff at 16.5 km and the CO profile are cutoff at 17.5 km, likely due to the aerosol in the plume causing problems with the solar occultation retrieval. The O_3 profile shows a negative anomaly relative to the background from 18.5 to 22.5 km. This low ozone anomaly was also seen in the ANSYO event and indicates O_3-poor tropospheric air displacing O_3-rich stratospheric air (Kablick et al., 2020; Khaykin et al., 2020). We note that vertical displacement of low O_3 may not be the only cause of the low O_3 anomaly. Analysis of the ANYSO event by Solomon et al. (2022) suggested that chemistry on the smoke particle surfaces may have contributed to reduced ozone. Further work is necessary to determine whether O_3 loss occurred for the Black Saturday event.

As further corroboration of trace gas anomalies, we also examined the MLS CO and HCN data. We first compiled all Southern Hemisphere profiles for 26–28 February 2009 and calculated the mean and standard deviation (σ) for CO and HCN at each retrieved pressure level. In Figures 12a and 12b we plot all profiles in the geographic range from 0° to 40°S, 20°E−120°E, color-coding in red profiles that deviate from the mean by at least 4.2σ anywhere in the altitude range 17–25 km. The choice of 4.2σ follows the practice used in Pumphrey et al. (2011). Also plotted in Figures 12a and 12b is the PV anomaly profile at the centroid position for 27 February 2009 (0000 UTC). The

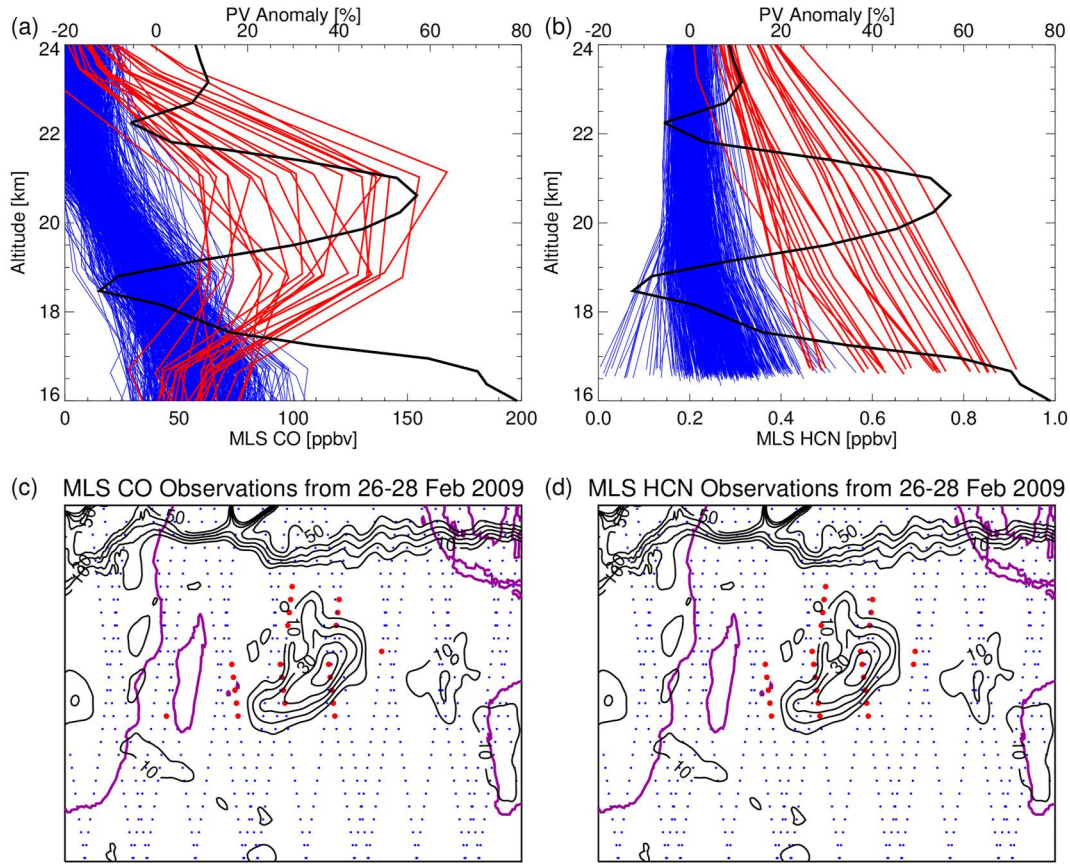

Figure 12. (a), (b) MLS CO and HCN profiles for 26–28 February 2009, color-coded by whether the individual profile deviates from the mean by at least 4.2σ (red if yes, blue if no). The black line is the PV anomaly profile at the centroid longitude and latitude. (c), (d) Maps of the PV anomaly for 27 February 2009 (in % with black contours) and the positions of the MLS profiles for 26–28 February 2009, color-coded by whether the individual (c) CO or (d) HCN profile deviates from the mean by at least 4.2σ (red if yes, blue if no). Coastlines are plotted in magenta.

CO profiles peak at similar altitude levels as the PV anomaly, and they show a broader maximum. The HCN profiles do not show a local peak due to the poor vertical resolution (∼10 km), but they do clearly show elevated levels associated with the SWIRL, as also demonstrated in Pumphrey et al. (2011). The locations of the >4.2σ profiles are plotted in Figures 12c and 12d along with the PV anomaly at the centroid level. There is a clear correspondence between high CO/HCN and high PV anomaly.

The temperature dipole structure continues into late February, as seen in the ERA5 temperature anomaly profile in Figure 2d. To corroborate the ERA5 results, we also show in Figure 2d a temperature anomaly profile from a COSMIC-1 GNSS-RO in the vicinity of the plume on 26 February (2100 UTC). The approximate location of this profile is indicated by a blue dot on Figure 10g. To calculate an anomaly for the GNSS-RO profile, we difference the profile with a smoothed profile using a boxcar filter with vertical width of ∼4 km (200 levels of ∼0.02 km). The GNSS-RO temperature anomaly shows a similar dipole pattern with warmer (colder) air below (above) the q' maximum. Compared with A20, this GNSS RO temperature anomaly of ∼6 K (∼8 K for ERA5) is about half that of the main ANYSO plume, which had peak dipole differences of ∼15 K.

4.4. 1–4 March

From 1 to 4 March, the SWIRL weakens further as it passes over the African continent, and eventually reaches its final demise. Figures 13a–13d shows the horizontal elongation as the SWIRL weakens and is sheared out by the ambient wind, and Figures 13e–13h shows the longitude/θ cross-sections indicating q' drops below the 30% threshold on 4 March. The demise of the SWIRL over Africa has similarities to the demise of the main ANSYO plume. Figure 4 of A20 shows that in late February–early March 2020 this SWIRL similarly moved westward

from Australia to Africa, and it was unable to be resolved in the anticyclone analysis on 3 March. However, it was tracked until 10 March by Kablick et al. (2020), and Khaykin et al. (2020) showed remnants of the ANSYO plume existed until early April. The ANSYO plume was at an altitude of ∼30 km rather than ∼21 km for the Black Saturday plume. In the next section, we use ECMWF forecasts to examine whether such a feature could be maintained using a forecast model in the absence of smoke-heating feedbacks included.

5. SWIRL Forecasts

While the dynamical signature of SWIRL is evident in the ERA5 reanalysis, the ability to forecast SWIRL dynamics requires smoke-related heating to be parameterized in the forecast model. Khaykin et al. (2020) showed that ECMWF forecasts were not able to maintain the vorticity anomalies associated with the ANYSO event. Similarly, A20 showed deficiencies in NAVGEM forecasts of one of the SWIRLs associated with the PNE event. Here, we examine two archived operational ECMWF forecasts of q' to determine how well they predicted the evolution of the Black Saturday SWIRL.

Figure 14 shows the analyzed and forecasted q' from 13 to 23 February, plotted at the centroid level for every 2 days. There are slight differences initially (compare Figures 14a–14g) due to the differences between the ERA5 reanalysis and the operational ECMWF analysis, but both versions clearly show the large positive q' north of New Zealand. Even after one day (not shown), there is evident weakening of the q' values and areal extent of $q' > 30\%$ in the forecast output. There is further deterioration of the SWIRL signature on 15 February, and from 17 to 23 February, the forecast no longer has any values of $q' > 30\%$ in the vicinity of the SWIRL. This result is consistent with the Khaykin et al. (2020) and A20 forecast/analysis comparisons and suggests that smoke heating is essential for maintaining the SWIRL dynamical signature, at least in these early days of its lifetime. We note that the analyses showed the position of this SWIRL rose from 412 to 470 K over this 10-day period, a heating rate of ∼5.8 K/day, providing additional confirmation of smoke-heating, which is not included in the forecast. This forecast "bust" provides circumstantial evidence that smoke-induced heating is necessary for creating and maintaining SWIRLs in global atmospheric models.

PV anomalies from an ECMWF forecast initialized 21 February are shown in Figure 15. Similar to 13 February, the strength of the forecasted q' is weaker than the analyzed values. This can be seen clearly from 25 to 27 February. Unlike the 13 February forecast, however, the SWIRL signature does not disappear as quickly; $q' > 30\%$ is still present even at six days (27 February). This is consistent with estimates of radiative timescales of 6–7 days given by Lestrelin et al. (2021) based on ERA5 heating rates for ANYSO and PNE plumes. The strength of the forecasted q' is weaker than the analyzed q', but the forecast tracks the shape and position of the SWIRL well even out to 8 days. This suggests that, at least from 25 February to 1 March, smoke-heating plays a smaller role, and PV evolution is more impacted from advection by the ambient flow. The overall heating rate of the SWIRL is slightly smaller during this 10-day period, ∼3.7 K/day, indicating less smoke-induced heating than from 13 to 23 February. Further simulations with radiative coupling, such as in Guimond et al. (2023), are necessary to elucidate cause and effect.

6. Summary and Conclusions

This study examined the SWIRL generated by the smoke plume injected into the stratosphere during the February 2009 Australian Black Saturday pyroCb outbreak. Clear dynamical signatures were evident in the ERA5 PV, which revealed anticyclonic rotation lasting for nearly three weeks accompanied by a vertical temperature dipole, rising motion, and transport over 27,000 km. The horizontal position of the SWIRL was confirmed with OMI aerosol index maps and the vertical position was confirmed with a GNSS-RO temperature profile, ACE-FTS solar occultation profiles of H_2O, CO, HCN, and O_3, MLS CO and HCN profiles, ACE imager aerosol extinction and CALIOP aerosol backscatter. The Black Saturday SWIRL was weaker in strength and duration than the primary SWIRL associated with ANYSO, but was likely on the same order as another ANYSO SWIRL (called "vortex 2" in Khaykin et al. (2020) and "P3" in Kablick et al. (2020)), which had a similar lifetime of about 3 weeks and similar rise in potential temperature (e.g., see the lower altitude PV anomaly in Figure 2a of Kablick et al., 2020). It was likely also on the same order as some of the SWIRLs accompanying PNE (Lestrelin et al., 2021).

The confinement of the elevated tracer and aerosol concentrations within the Black Saturday SWIRL was similar to what was seen for ANYSO. In both cases, the anticyclone prevented the naturally occurring shearing and dispersive properties from removing the anomalies. This process enhances the stratospheric residence time of the

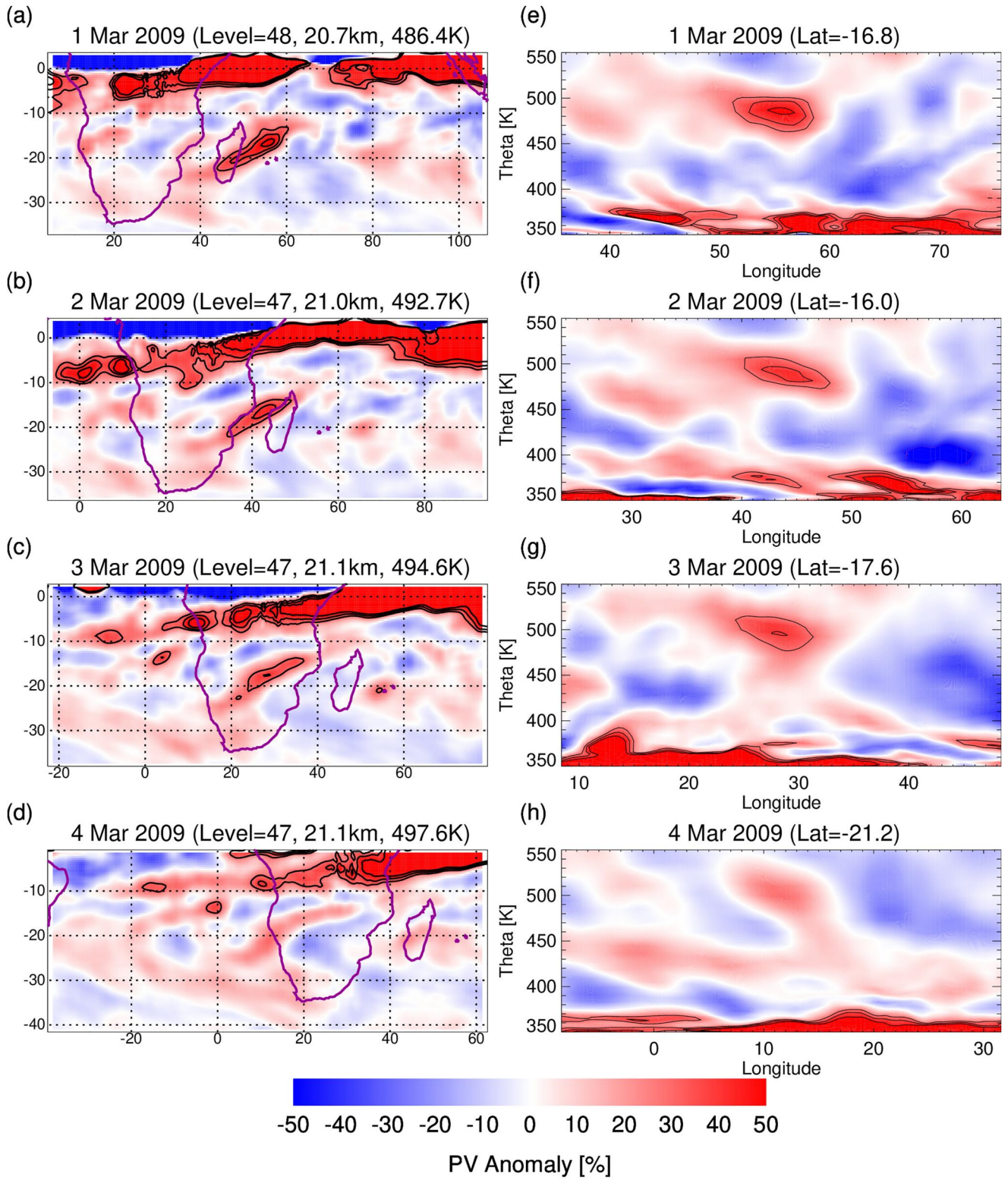

Figure 13. (a)–(d) ERA5 PV anomaly maps for 1–4 March 2009 (0000 UTC for each case) at the centroid model level for each time. Altitude and θ at the centroid location are provided. Black contours are values of 30%, 40%, and 50%. (e)–(h) ERA5 PV anomaly as a function of longitude and potential temperature for 1–4 March 2009 (0000 UTC in each case) at the centroid latitude for each date. Black contours are values of 30%, 40%, and 50%.

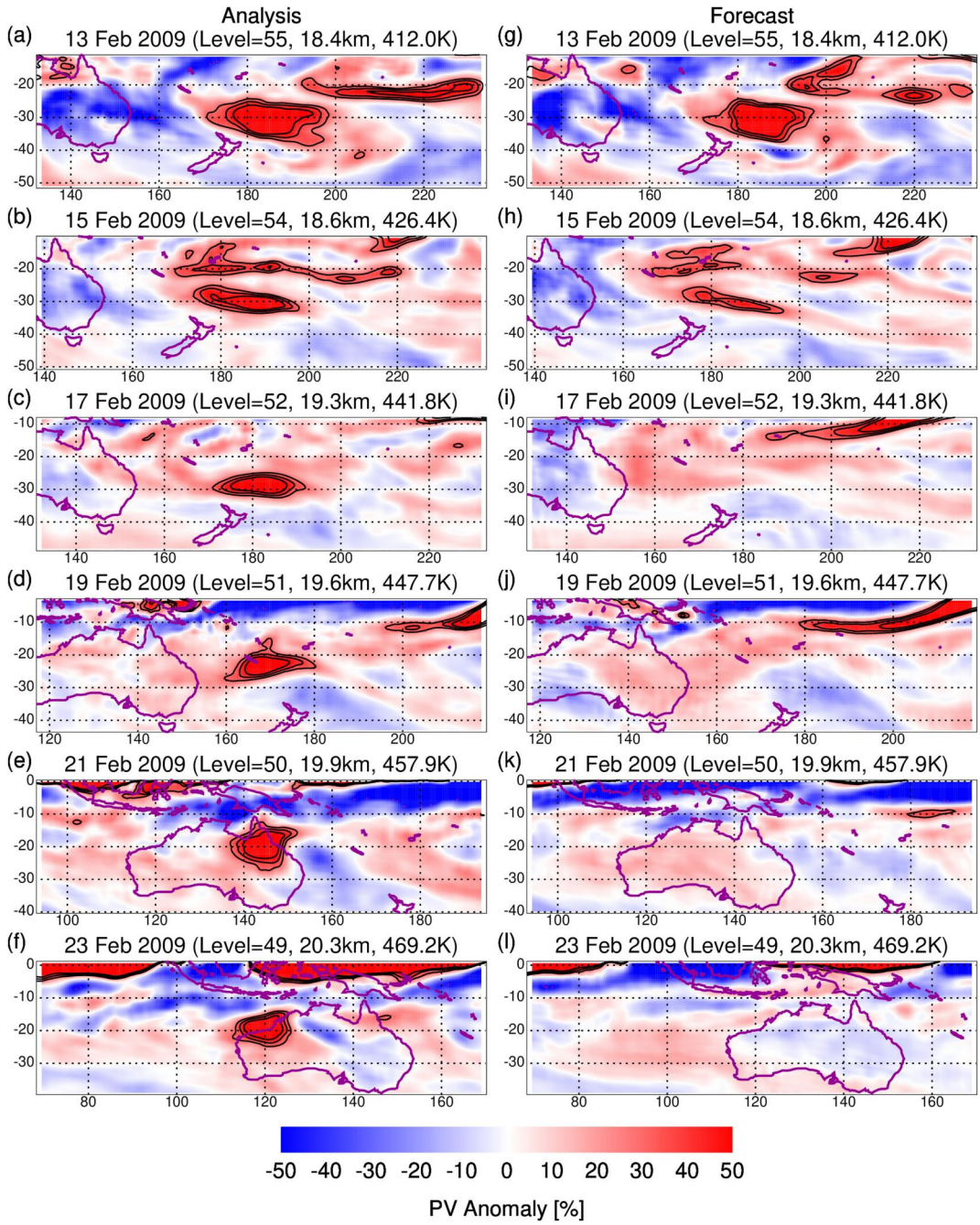

Figure 14. (a)–(f) ERA5 PV anomaly maps on 13, 15, 17, 19, 21, and 23 February 2009 (0000 UTC for each case) at the centroid model level for each time. (g)–(l) ECMWF operational forecast (initialized 13 February 2009 at 0000 UTC) maps of PV anomaly at 13, 15, 17, 19, 21, and 23 February 2009 (0000 UTC for each case) at the centroid model level for each time. Black contours are values of 30%, 40%, and 50%. Altitude and θ at the centroid location are provided.

wildfire emissions, with potential climate implications. Shah and Haynes (2023) discuss the impacts of vortex stripping and dispersion of the tracer by the large-scale flow in the context of an axisymmetric model. More detailed three dimensional Lagrangian modeling efforts by Curbelo and Rypina (2023) were performed for SWIRLs associated with the ANYSO event. They showed that while most particles remain in the anticyclone, some leaked out along the unstable manifold. These stretched into large filaments and then mixed rapidly with

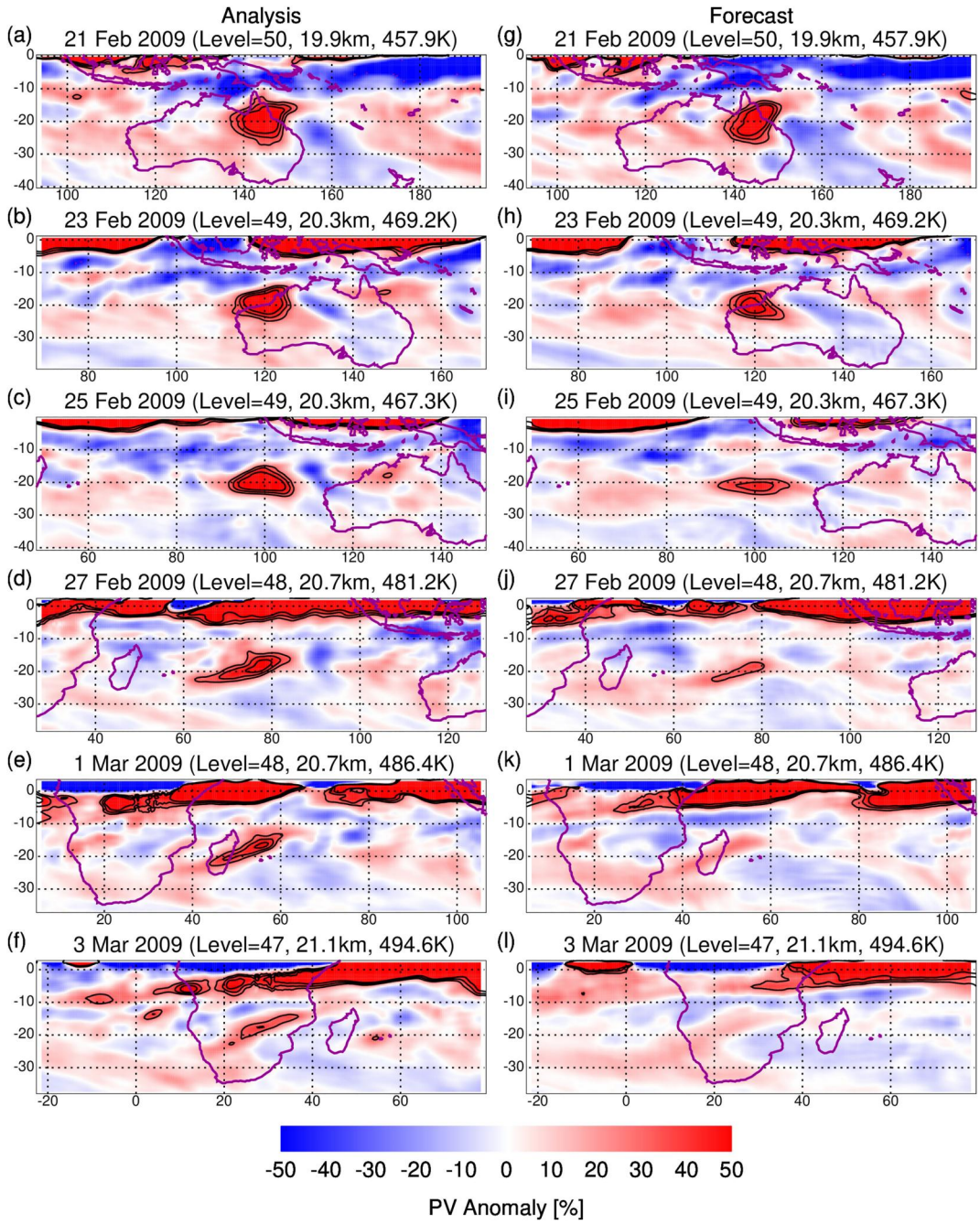

Figure 15. (a)–(f) ERA5 PV anomaly maps on 21, 23, 25, and 27 February and 1 and 3 March 2009 (0000 UTC for each case) at the centroid model level for each time. (g)–(l) ECMWF operational forecast (initialized 21 February 2009 at 0000 UTC) maps of PV anomaly on 21, 23, 25, and 27 February and 1 and 3 March 2009 (0000 UTC for each case) at the centroid model level for each time. Black contours are values of 30%, 40%, and 50%. Altitude and θ at the centroid location are provided.

surrounding air. This is consistent with observational analysis from Khaykin et al. (2020) and Lestrelin et al. (2021), who showed evidence of leakage using CALIOP data.

Two operational ECMWF forecasts were examined during the early and late periods of the Black Saturday SWIRL. The early forecast failed to simulate the SWIRL beyond ~3 days, indicating the need for including smoke radiative heating in numerical weather prediction models. The later forecast maintained a PV anomaly signature out to ~8 days, although at a weaker extent than seen in the analyses. It is clear from this and previous

analysis/forecast comparisons that the lack of smoke-heating in forecast models significantly limits accurate prediction of downstream impacts from these events. Similar stratospheric forecast deficiencies were seen in the ANSYO event (Khaykin et al., 2020), while broader-scale tropospheric weather impacts due to wildfires are also being studied (e.g., Zhang et al., 2022).

This study of the Black Saturday event adds to the cases examined for smoke-induced dynamical anomalies. SWIRLs have now been documented in the three largest pyroCb outbreaks on record (Black Saturday, PNE, and ANYSO). It is likely that examination of other historical pyroCb events will reveal additional SWIRLs that can add to our knowledge of these newly-discovered weather features. The recent Canadian pyroCb outbreaks in the summer of 2023, for example, include evidence of dynamical perturbations. However, it remains to be seen the extent to which SWIRLs occur in smaller pyroCb outbreaks and whether they are detectable in meteorological analyses, particularly in the pre-satellite era (prior to 1979), where sufficient data for analyzing SWIRLS may not be available.

In addition to smoke-induced dynamics, recent work has shown that volcanic sulfate plumes can result in dynamical perturbations including self-lofting and anticyclonic rotation, a phenomenon coined as a Vorticized Volcanic Plume (VVP) (Khaykin et al., 2022). SWIRLs and VVPs, along with Dust-Infused Baroclinic Storms (DIBS, Fromm et al., 2016), could be considered as subsets of a larger grouping of aerosol-induced dynamical anomalies (we suggest AIDA as a new acronym to describe this larger group). The importance of these phenomena for both climate research and for numerical weather prediction is becoming ever clearer as new discoveries are being made.

Data Availability Statement

The OMI and MLS data used in this effort were acquired as part of the activities of NASA's Science Mission Directorate and are archived and distributed by the Goddard Earth Sciences (GES) Data and Information Services Center (DISC), https://disc.gsfc.nasa.gov. ACE-FTS data were obtained from https://doi.org/10.20383/101.0291. COSMIC-1 data are available at the CDAAC. We use the 2021 reprocessed data https://data.cosmic.ucar.edu/gnss-ro/cosmic1/repro2021/level2/2009/057. CALIOP data are available at https://doi.org/10.5067/CALIOP/CALIPSO/CAL_LID_L1-Standard-V4-51. ECMWF data are published under a Creative Commons Attribution 4.0 International (CC BY 4.0). https://creativecommons.org/licenses/by/4.0. ECMWF does not accept any liability whatsoever for any error or omission in the data, their availability, or for any loss or damage arising from their use. ERA5 data were obtained using the ECMWF MARS system to access the ERA5 Catalogue. https://apps.ecmwf.int/data-catalogues/era5/?class=ea. ECMWF operational analyses were obtained using the MARS system to access the Archive Catalogue. https://apps.ecmwf.int/archive-catalogue/?class=od. Further information is available at www.ecmwf.int. © 2023 European Centre for Medium-Range Weather Forecasts (ECMWF).

Acknowledgments
This work was funded by the U. S. Naval Research Laboratory 6.1 and 6.2 Base Programs. Additional support for David Peterson was provided by the NASA's Modeling, Analysis, and Prediction (MAP) Program (80HQTR21T0099), and additional support for George Kablick and Michael Fromm was provided by the NASA's Aura Science Team (80HQTR20T0052). The Atmospheric Chemistry Experiment (ACE), also known as SCISAT, is a Canadian-led mission mainly supported by the Canadian Space Agency. We appreciate helpful conversations with Chris Boone regarding the ACE data.

References

Allen, D. R., Fromm, M. D., Kablick, G. P., III, & Nedoluha, G. E. (2020). Smoke With Induced Rotation and Lofting (SWIRL) in the stratosphere. *Journal of the Atmospheric Sciences*, *77*(12), 4297–4316. https://doi.org/10.1175/JAS-D-20-0131.1

Andrews, D. G., Holton, J. R., & Leovy, C. B. (1987). *Middle atmosphere dynamics* (p. 489). Academic Press.

Bernath, P. F., Steffen, J., Crouse, J., & Boone, C. D. (2020). Sixteen-year trends in atmospheric trace gases from orbit. *Journal of Quantitative Spectroscopy and Radiative Transfer*, *253*, 107178. https://doi.org/10.1016/j.jqsrt.2020.107178

Bhartia, P. K. (2012). *OMI/Aura TOMS-like ozone, aerosol index, cloud radiance fraction L3 1 day 1 degree x 1 degree V3, NASA Goddard Space Flight Center*. Goddard Earth Sciences Data and Information Services Center (GES DISC). https://doi.org/10.5067/Aura/OMI/DATA3001

Boone, C. D., Bernath, P. F., Cok, D., Jones, S. C., & Steffen, J. (2020). Version 4 retrievals for the atmospheric chemistry experiment Fourier transform spectrometer (ACE-FTS) and imagers. *Journal of Quantitative Spectroscopy and Radiative Transfer*, *247*, 106939. https://doi.org/10.1016/j.jqsrt.2020.106939

Boone, C. D., Bernath, P. F., & Fromm, M. D. (2020). Pyrocumulonimbus stratospheric plume injections measured by the ACE-FTS. *Geophysical Research Letters*, *47*(15), e2020GL088442. https://doi.org/10.1029/2020GL088442

Boone, C. D., Bernath, P. F., & Lecours, M. (2023). Version 5 retrievals for ACE-FTS and ACE-imagers. *Journal of Quantitative Spectroscopy & Radiative Transfer*, *310*(210), 108749. https://doi.org/10.1016/j.jqsrt.2023.108749

Curbelo, J., & Rypina, I. I. (2023). A three dimensional Lagrangian analysis of the smoke plume from the 2019/2020 Australian wildfire event. *Journal of Geophysical Research: Atmospheres*, *128*(21), e2023JD039773. https://doi.org/10.1029/2023JD039773

Das, S., Colarco, P. R., Oman, L. D., Taha, G., & Torres, O. (2021). The long-term transport and radiative impacts of the 2017 British Columbia pyrocumulonimbus smoke aerosols in the stratosphere. *Atmospheric Chemistry and Physics*, *21*(15), 12069–12090. https://doi.org/10.5194/acp-21-12069-2021

de Laat, A. T. J., Stein Zweers, D., Boers, R., & Tuinder, O. N. E. (2012). A solar escalator: Observational evidence of the self-lifting of smoke and aerosols by absorption of solar radiation in the February 2009 Australian Black Saturday plume. *Journal of Geophysical Research*, *117*(D4), D04204. https://doi.org/10.1029/2011jd017016

Doglioni, G., Aquila, V., Das, S., Colarco, P. R., & Zardi, D. (2022). Dynamical perturbation of the stratosphere by a pyrocumulonimbus injection of carbonaceous aerosols. *Atmospheric Chemistry and Physics*, *17*, 11049–11064. https://doi.org/10.5194/acp-22-11049-2022

Fromm, M., Kablick, G., III, & Caffrey, P. (2016). Dust-infused baroclinic cyclone storms clouds: The evidence, meteorology, and some implications. *Geophysical Research Letters*, *43*(24), 12643–12650. https://doi.org/10.1002/2016GL071801

Fromm, M. D., Kablick, G. P., Peterson, D. A., Kahn, R. A., Flower, V. J. B., & Seftor, C. J. (2021). Quantifying the source term and uniqueness of the August 12, 2017 Pacific Northwest pyroCb event. *J. Geophys. Res.: Atm.*, *126*(13), e2021JD034928. https://doi.org/10.1029/2021JD034928

Glatthor, N., Höpfner, M., Semeniuk, K., Lupu, A., Palmer, P. I., McConnell, J. C., et al. (2013). The Australian bushfires of February 2009: MIPAS observations and GEM-AQ model results. *Atmospheric Chemistry and Physics*, *13*(3), 1637–1658. https://doi.org/10.5194/acp-13-1637-2013

Guimond, S. R., Reisner, J., & Dubey, M. (2023). The dynamics of megafire smoke plumes in climate models: Why a converged solution matters for physical interpretations. *Journal of Advances in Modeling Earth Systems*, *15*(4), e2022MS003432. https://doi.org/10.1029/2022MS003432

Hershbach, H., Bell, B., Berrisford, P., Hirahara, S., Horányi, A., Muñoz-Sabater, J., et al. (2020). The ERA5 global reanalysis. *Quarterly Journal of the Royal Meteorological Society*, *146*(730), 1999–2049. https://doi.org/10.1002/qj.3803

Kablick, G. P., III, Allen, D. R., Fromm, M. D., & Nedoluha, G. E. (2020). Australian pyroCb smoke generates synoptic-scale stratospheric anticyclones. *Geophysical Research Letters*, *47*(13). https://doi.org/10.1029/2020GL088101

Khaykin, S., Legras, B., Bucci, S., Sellitto, P., Isaksen, L., Tencé, F., et al. (2020). The 2019/20 Australian wildfires generated a persistent smoke-charged vortex rising up to 35 km altitude. *Commun. Earth Environ*, *1*, 22. https://doi.org/10.1038/s43247-020-00022-5

Khaykin, S. M., de Laat, A. T. J., Godin-Beekmann, S., Hauchecorne, A., & Ratynski, M. (2022). Unexpected self-lofting and dynamical confinement of volcanic plumes: The Raikoke 2019 case. *Nature Scientific Reports*, *12*(1), 22409. https://doi.org/10.1038/s41598-022-27021-0

Khaykin, S. M., Godin-Beekmann, S., Hauchecorne, A., Pelon, J., Ravetta, F., & Keckhut, P. (2018). Stratospheric smoke with unprecedentedly high backscatter observed by lidar above southern France. *Geophysical Research Letters*, *45*(3), 1639–1646. https://doi.org/10.1002/2017GL076763

Lestrelin, H., Legras, B., Podglajen, A., & Salihoglu, M. (2021). Smoke-charged vortices in the stratosphere generated by wildfires and their behaviour in both hemispheres: Comparing Australia 2020 to Canada 2017. *Atmospheric Chemistry and Physics*, *21*(9), 7113–7134. https://doi.org/10.5194/acp-21-7113-2021

Livesey, N. J., Read, W. G., Wagner, P. A., Froidevaux, L., Lambert, A., Manney, G. L., et al. (2020). *Earth observing system (EOS) Aura Microwave Limb Sounder (MLS) version 4.2x level 2 and 3 data quality and description document*. In *Tech. Rep. JPL D-33509 Rev E*. NASA Jet Propulsion Laboratory California Institute of Technology. Retrieved from https://mls.jpl.nasa.gov/data/v4-2_data_quality_document.pdf

Pumphrey, H. C., Filipiak, M. J., Livisey, N. J., Schwartz, M. J., Boone, C., Walker, K. A., et al. (2007). Validation of middle-atmosphere carbon monoxide retrievals from the Microwave Limb Sounder on Aura. *Journal of Geophysical Research*, *112*(D24), D24S38. https://doi.org/10.1029/2007JD008723

Pumphrey, H. C., Jimenez, C. J., & Waters, J. M. (2006). Measurement of HCN in the middle atmosphere by EOS MLS. *Geophysical Research Letters*, *33*(8), L08804. https://doi.org/10.1029/2005GL025656

Pumphrey, H. C., Santee, M. L., Livesey, N. J., Schwartz, M. J., & Read, W. G. (2011). Microwave Limb Sounder observations of biomass-burning products from the Australian bush fires of February 2009. *Atmospheric Chemistry and Physics*, *11*(13), 6285–6296. https://www.doi.org/10.5194/acp-11-6285-2001

Schwartz, M. J., Santee, M. L., Pumphrey, H. C., Manney, G. L., Lambert, A., Livesey, N. J., et al. (2020). Australian New Year's pyroCb impact on stratospheric composition. *Geophysical Research Letters*, *47*(24), e2020GL090831. https://doi.org/10.1029/2020GL090831

Shah, K. S., & Haynes, P. H. (2023). How heating tracers drive self-lofting long-lived stratospheric anticyclones: Simple dynamical models [preprint]. EGUsphere https://doi.org/10.5194/egusphere-2023-2265

Siddaway, J. M., & Petelina, S. V. (2011). Transport and evolution of the 2009 Australian Black Saturday bushfire smoke in the lower stratosphere observed by OSIRIS on Odin. *Journal of Geophysical Research*, *116*(D6), D06203. https://www.doi.org/10.1029/2010jd015162

Solomon, S., Dube, K., Stone, K., Yu, P., Kinnison, D., Toon, O. B., et al. (2022). On the stratospheric chemistry of midlatitude wildfire smoke. *Proceedings of the National Academy of Sciences*, *119*(10), e2117325119. https://doi.org/10.1073/pnas.2117325119

Torres, O., Bhartia, P. K., Jethva, H., & Ahn, C. (2018). Impact of the ozone monitoring instrument row anomaly on the long-term record of aerosol products. *Atmospheric Measurement Techniques*, *11*(5), 2701–2715. https://doi.org/10.5194/amt-11-2701-2018

Torres, O., Bhartia, P. K., Taha, G., Jethva, H., Das, S., Colarco, P., et al. (2020). Stratospheric injection of massive smoke plume from Canadian boreal fires in 2017 as seen by DSCOVR-EPIC, CALIOP, and OMPS-LP observations. *Journal of Geophysical Research: Atmospheres*, *125*(10), e2020JD032579. https://doi.org/10.1029/2020JD032579

Torres, O., Tanskanen, A., Veihelman, B., Ahn, C., Braak, R., Bhartia, P. K., et al. (2007). Aerosols and surface UV products from OMI observations: An overview. *Journal of Geophysical Research*, *112*(D24), D24S47. https://doi.org/10.1029/2007JD008809

UCAR COSMIC Program. (2022). COSMIC-1 Data Products [Dataset]. UCAR/NCAR - COSMIC https://doi.org/10.5065/ZD80-KD74

Winker, D., Vaughan, M., Omar, A., Hu, Y., Powell, K., Liu, Z., et al. (2009). Overview of the CALIPSO mission and CALIOP data processing algorithms. *Journal of Atmospheric and Oceanic Technology*, *26*(11), 2310–2323. https://doi.org/10.1175/2009JTECHA1281.1

Yu, P., Toon, O. B., Bardeen, C. G., Zhu, Y., Rosenlof, K. H., Portmann, R. W., et al. (2019). Black carbon lofts wildfire smoke high into the stratosphere to form a persistent plume. *Science*, *365*(6453), 587–590. https://doi.org/10.1126/science.aax1748

Zhang, Y., Fan, J., Shrivastava, M., Homeyer, C. R., Wang, Y., & Seinfeld, J. H. (2022). Notable impact of wildfires in the western United States on weather hazards in the central United States. *Proceedings of the National Academy of Sciences*, *119*(44), e2207329119. https://doi.org/10.1073/pnas.2207329119